Multi-Grain Crystallography

Jonathan Wright

ESRF | The European Synchrotron

Overview

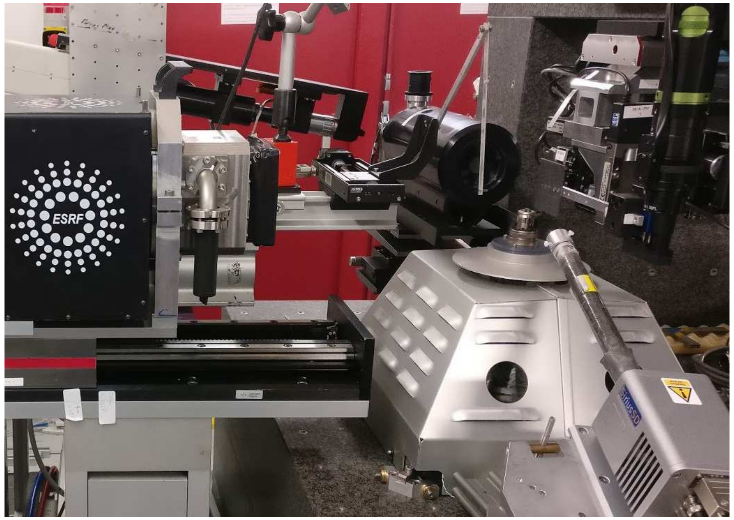

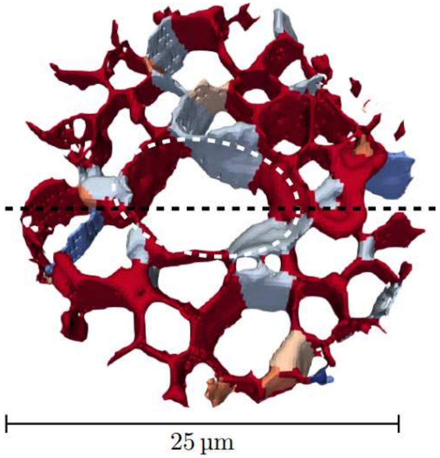

ESRF and ID11

Diffraction / 3DXRD / Grain Mapping

Diffraction Tomography

Machine commissioning : 2 Dec 2019 … Beamlines: March 2020

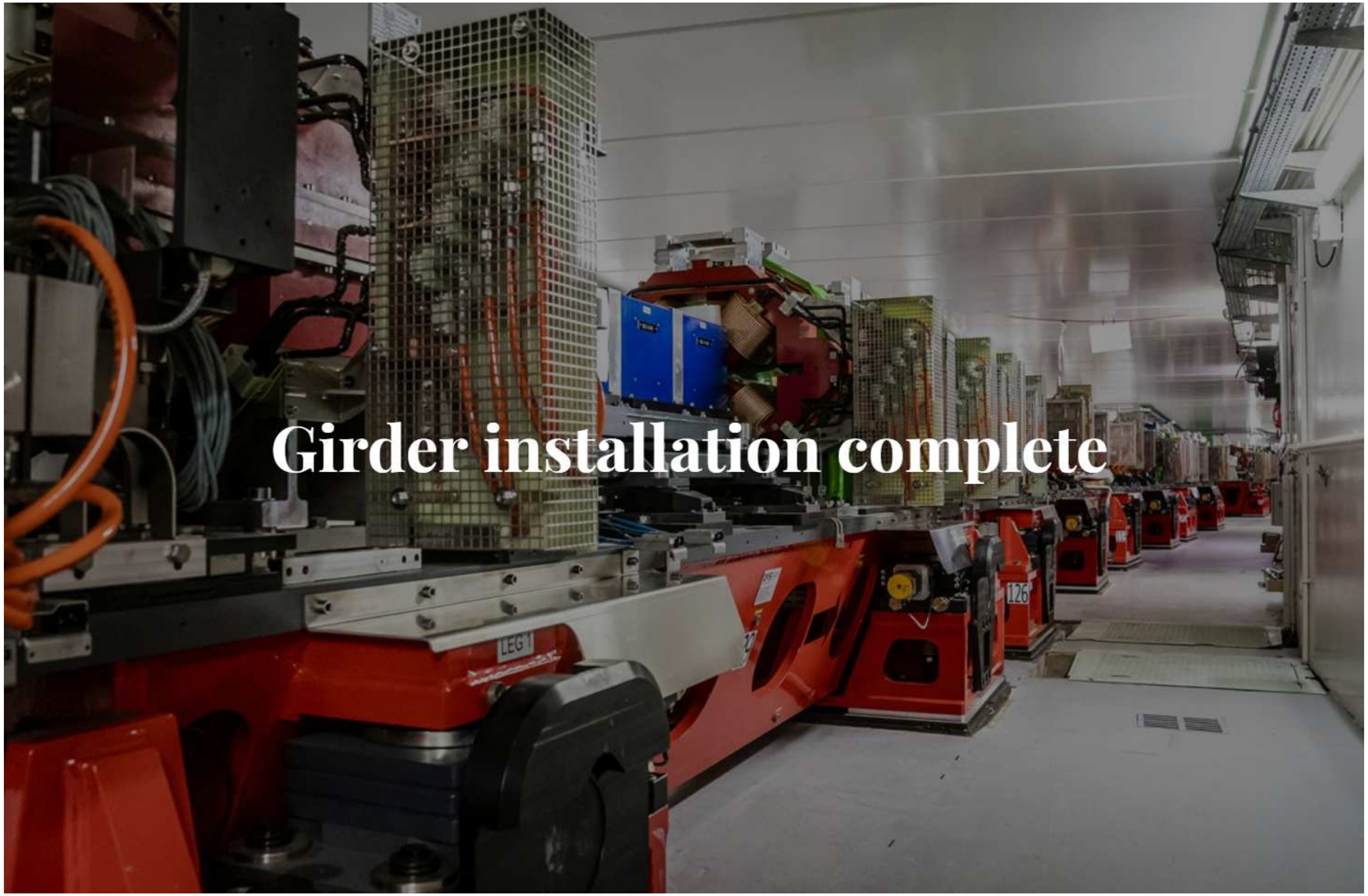

ESRF Upgrade Phase II : new machine in 2019-2020

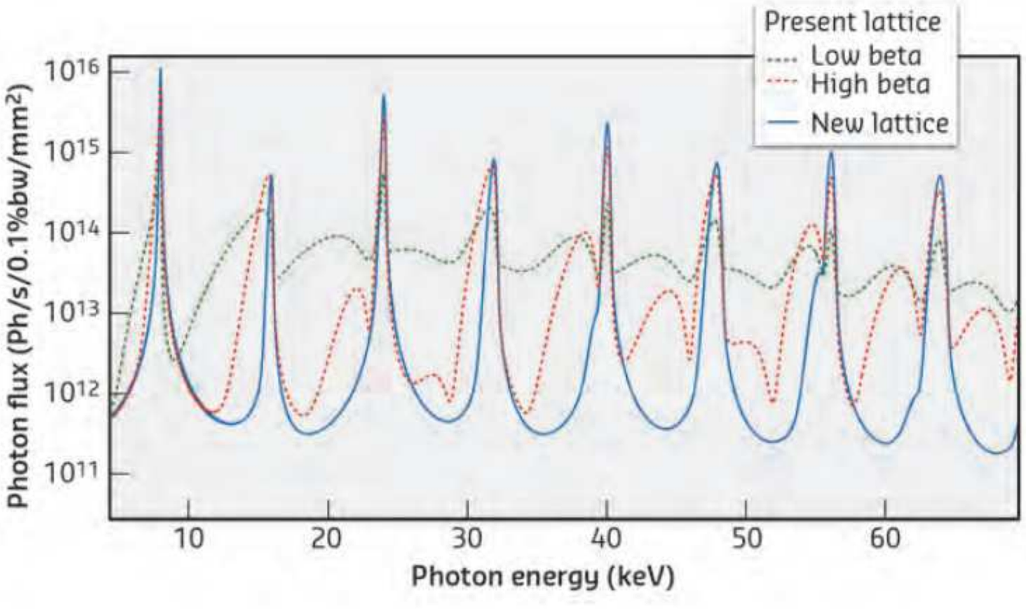

~40X more photons for ID11 optics

Cleaner spectrum

What is multi-grain crystallography ?

Spotty diffraction patterns : more than 1 crystal but no powder average

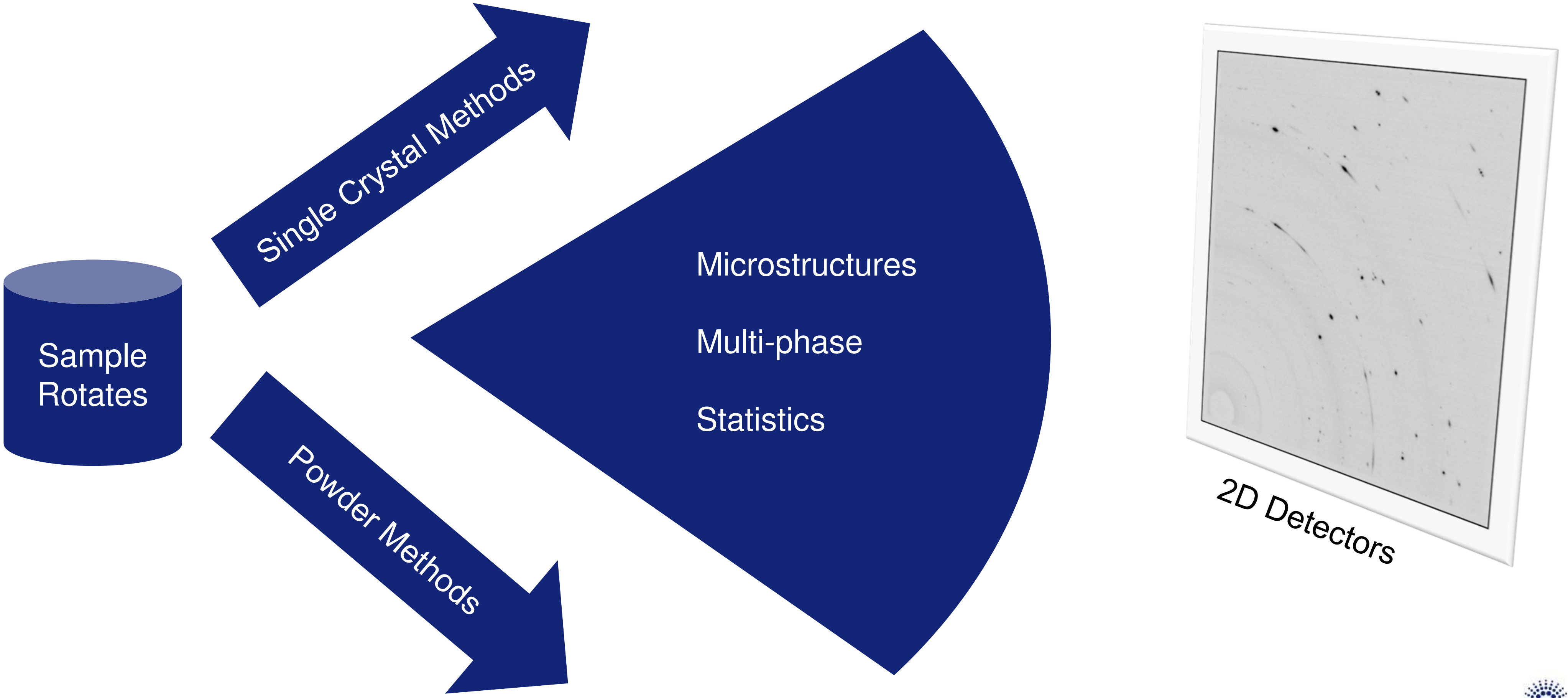

Sample Rotates

Single Crystal Methods

Powder Methods

Microstructures

Multi-phase

Statistics

2D Detectors

Single Crystal

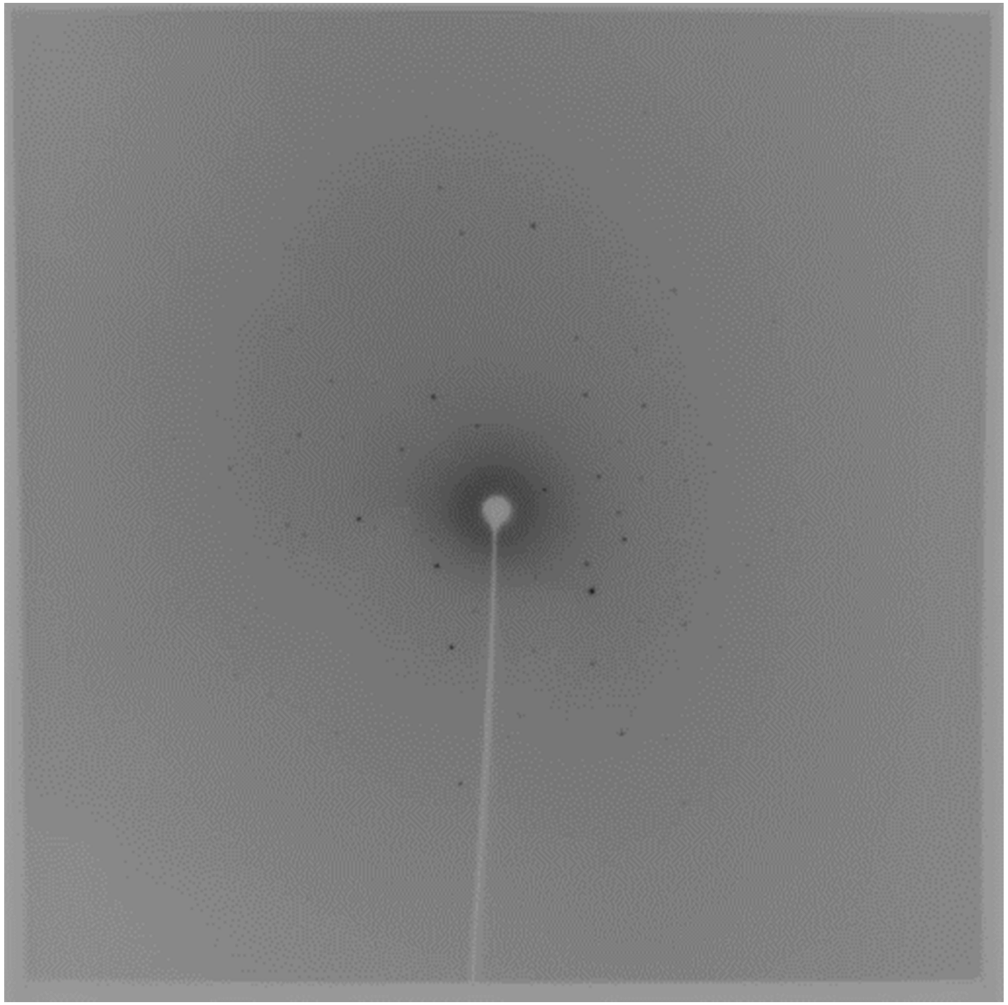

Many Crystals

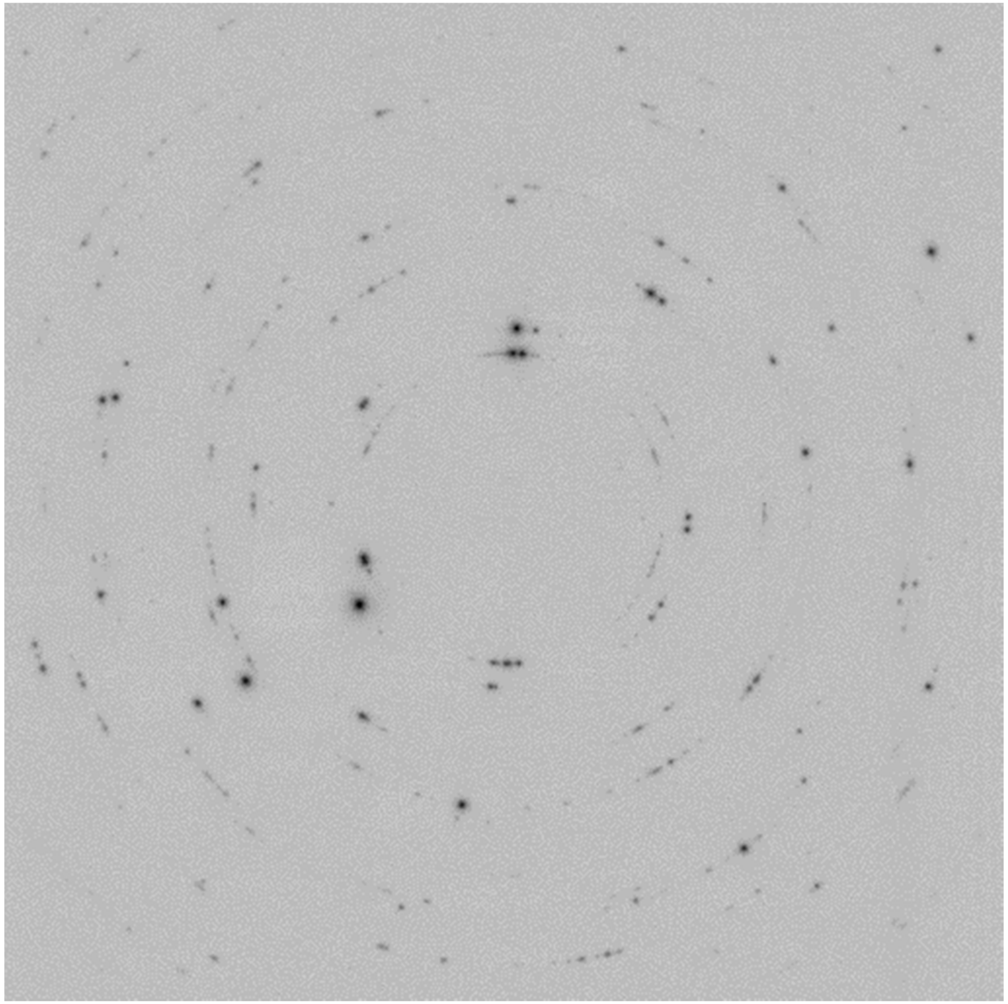

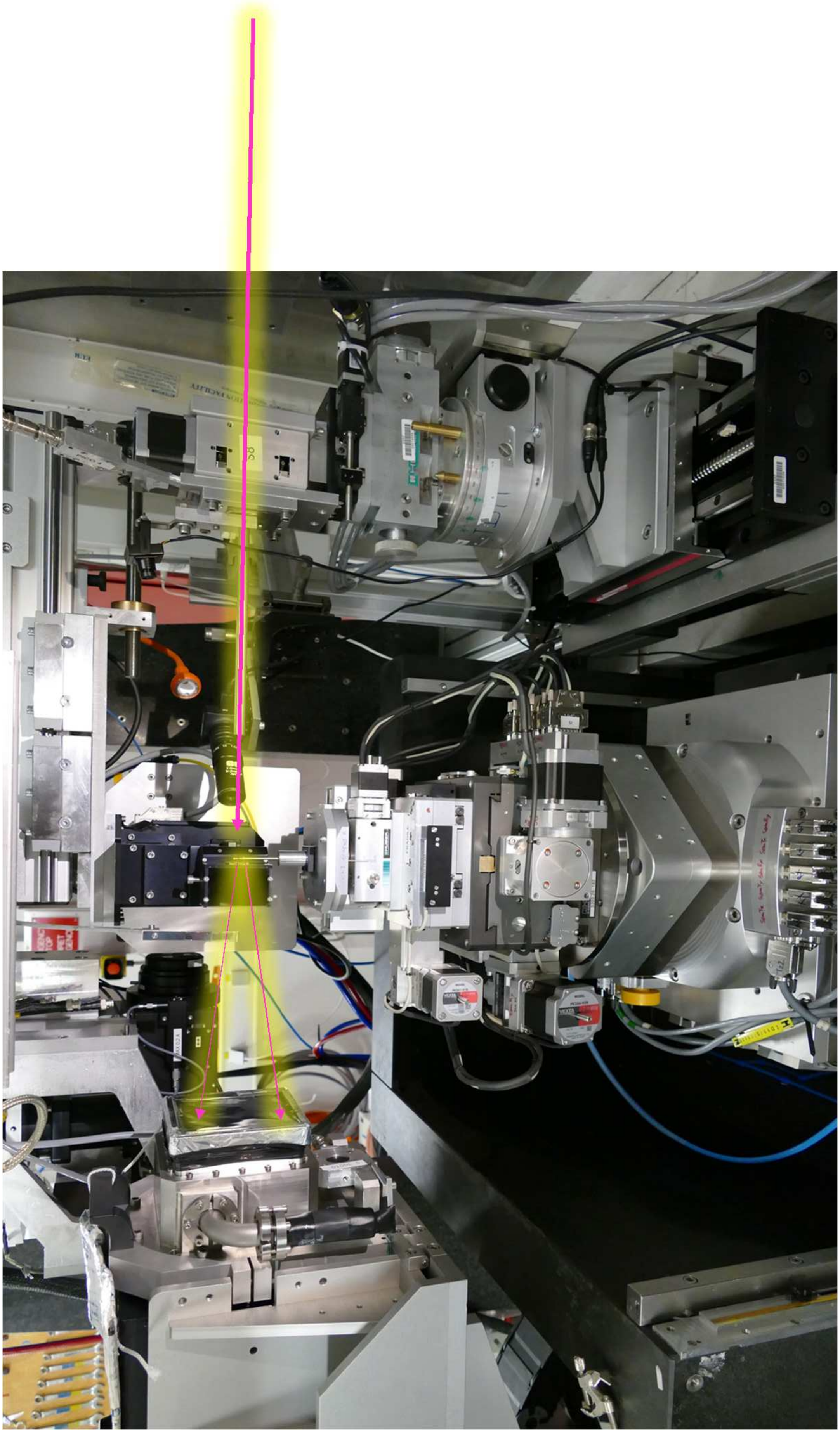

Structures from tiny crystals

Figure 1. a) Photograph of powderous $Pb_2Si_5N_8$; b) Brightfield TEM image of the single crystal used for single-crystal X-ray diffraction (XRD).

Communications
Angewandte Chemie

Lead Nitride

International Edition: DOI: 10.1002/anie.201812457
German Edition: DOI: 10.1002/ange.201812457

Cationic Pb_2 Dumbbells Stabilized in the Highly Covalent Lead Nitridosilicate $Pb_2Si_5N_8$

Philipp Bielec, Ryky Nelson, Ralf P. Stoffel, Lucien Eisenburger, Daniel Günther, Ann-Kathrin Henß, Jonathan P. Wright, Oliver Oeckler, Richard Dronskowski, and Wolfgang Schnick**

$R_1 = 2.3\%$

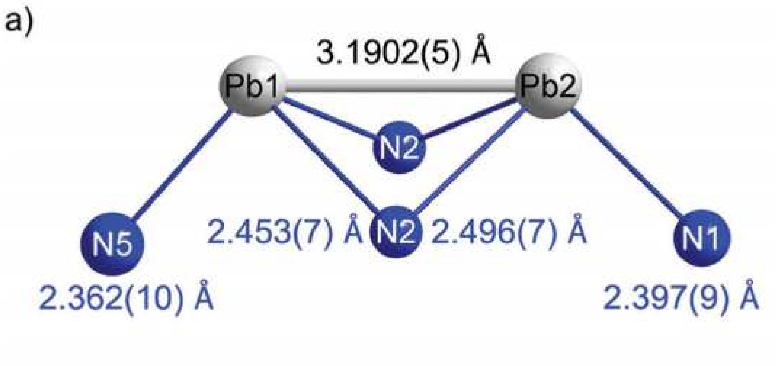

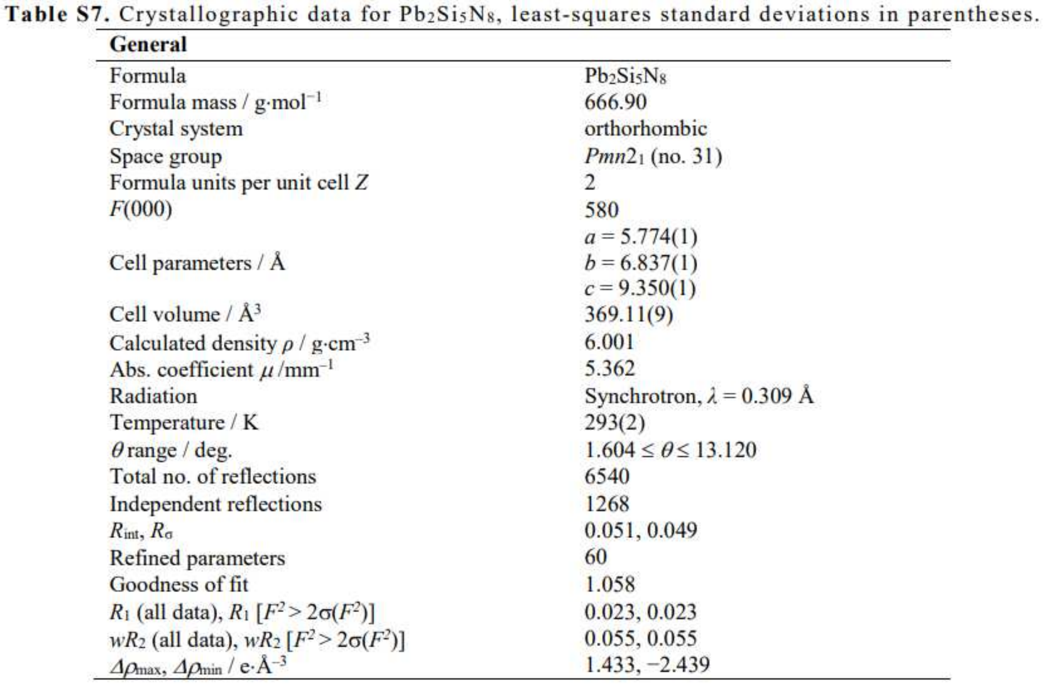

Table S7. Crystallographic data for $Pb_2Si_5N_8$, least-squares standard deviations in parentheses.

General	
Formula	$Pb_2Si_5N_8$
Formula mass / g·mol^{-1}	666.90
Crystal system	orthorhombic
Space group	$Pmn2_1$ (no. 31)
Formula units per unit cell Z	2
$F(000)$	580
Cell parameters / Å	$a = 5.774(1)$ $b = 6.837(1)$ $c = 9.350(1)$
Cell volume / Å^3	369.11(9)
Calculated density ρ / g·cm^{-3}	6.001
Abs. coefficient μ /mm^{-1}	5.362
Radiation	Synchrotron, $\lambda = 0.309$ Å
Temperature / K	293(2)
θ range / deg.	$1.604 \leq \theta \leq 13.120$
Total no. of reflections	6540
Independent reflections	1268
R_{int}, R_σ	0.051, 0.049
Refined parameters	60
Goodness of fit	1.058
R_1 (all data), R_1 $[F^2 > 2\sigma(F^2)]$	0.023, 0.023
wR_2 (all data), wR_2 $[F^2 > 2\sigma(F^2)]$	0.055, 0.055
$\Delta\rho_{max}$, $\Delta\rho_{min}$ / e·Å^{-3}	1.433, −2.439

New station added to ID11

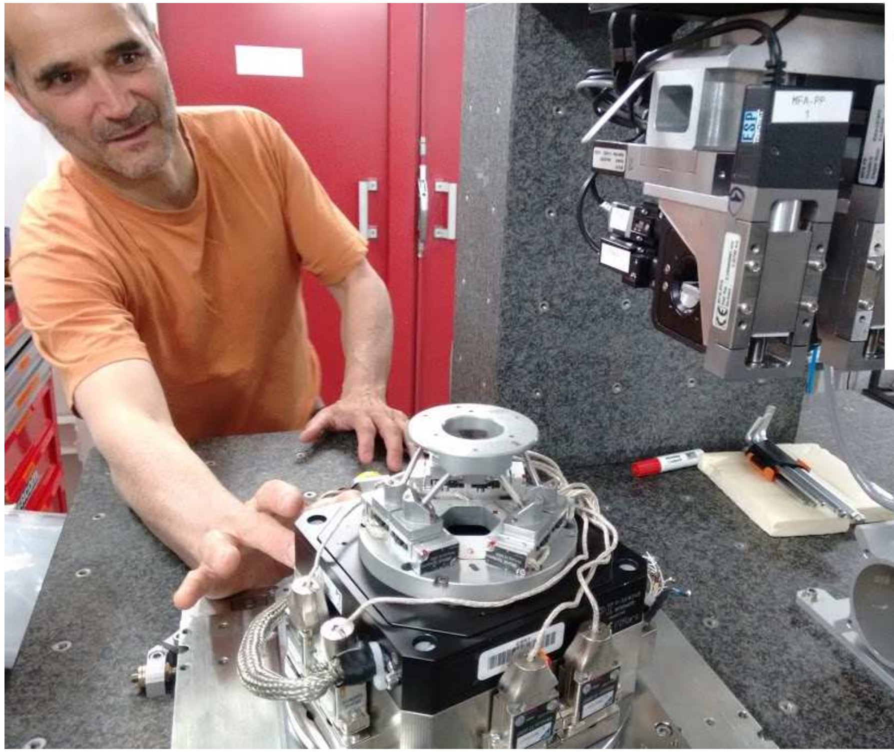

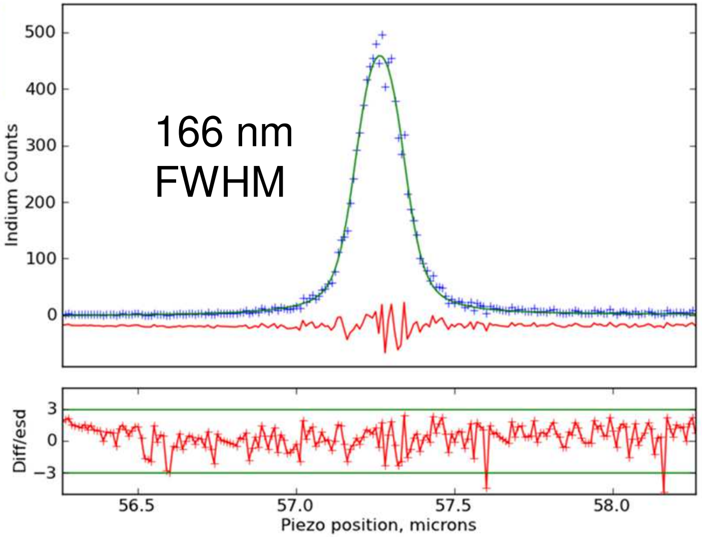

166 nm
FWHM

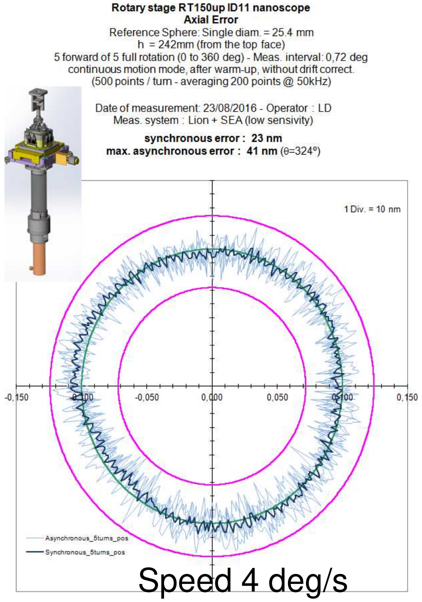

Rotary stage RT150up ID11 nanoscope
Axial Error
Reference Sphere: Single diam. = 25.4 mm
h = 242mm (from the top face)
5 forward of 5 full rotation (0 to 360 deg) - Meas. interval: 0,72 deg
continuous motion mode, after warm-up, without drift correct.
(500 points / turn - averaging 200 points @ 50kHz)

Date of measurement: 23/08/2016 - Operator : LD
Meas. system : Lion + SEA (low sensivity)

synchronous error : 23 nm
max. asynchronous error : 41 nm (θ=324°)

41 nm!

Speed 4 deg/s

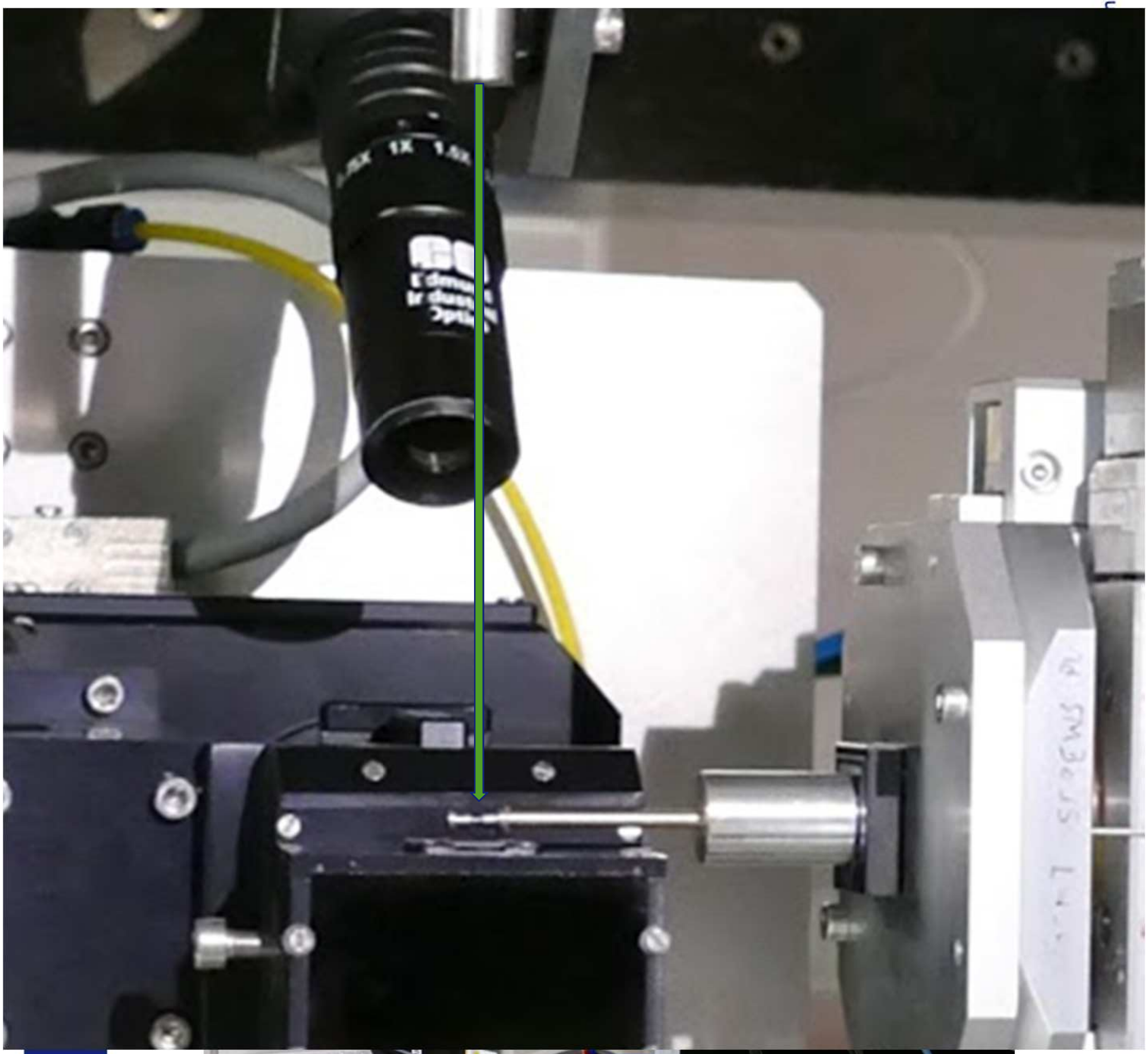

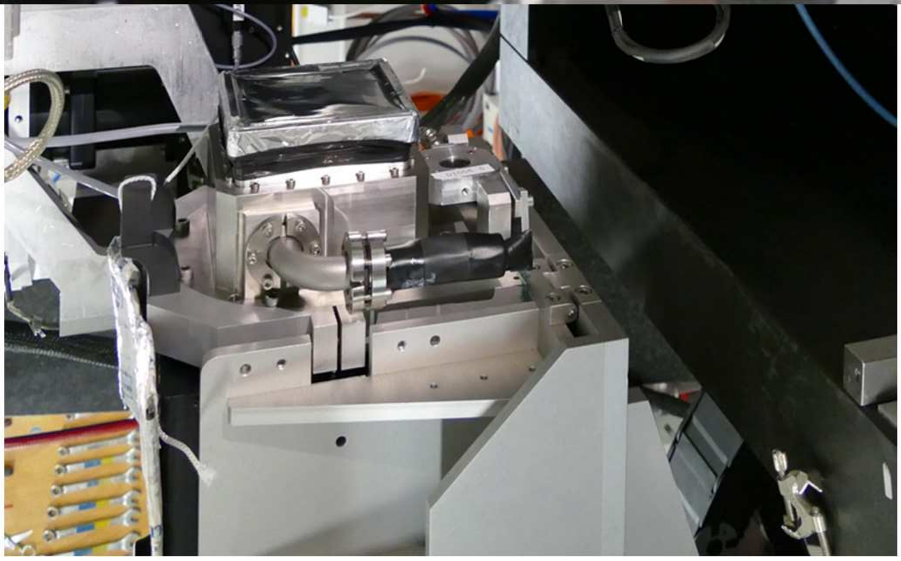

Near-field and far-field detectors

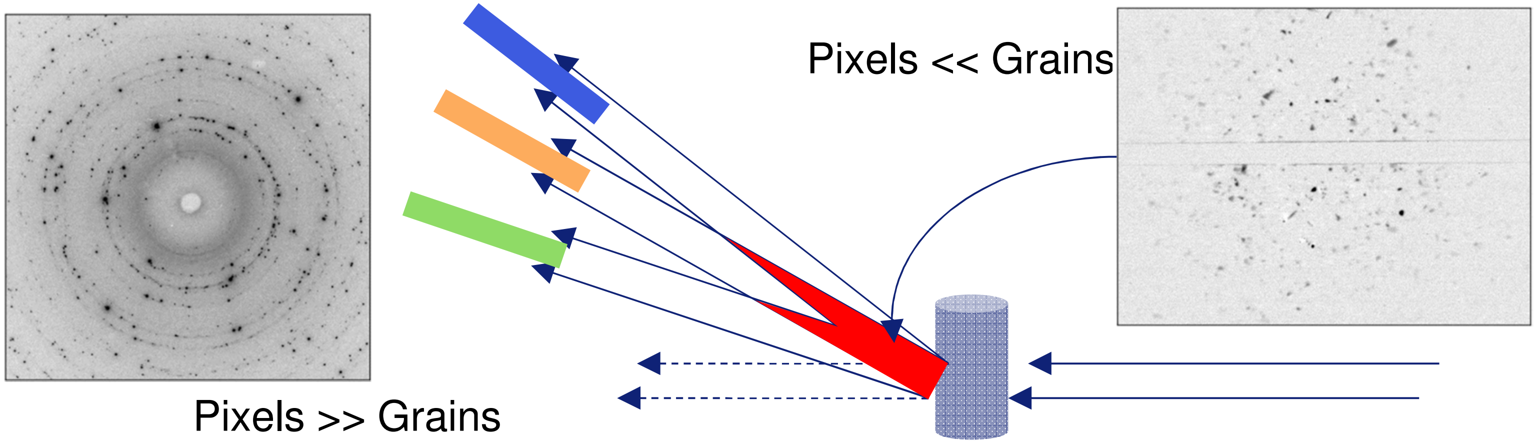

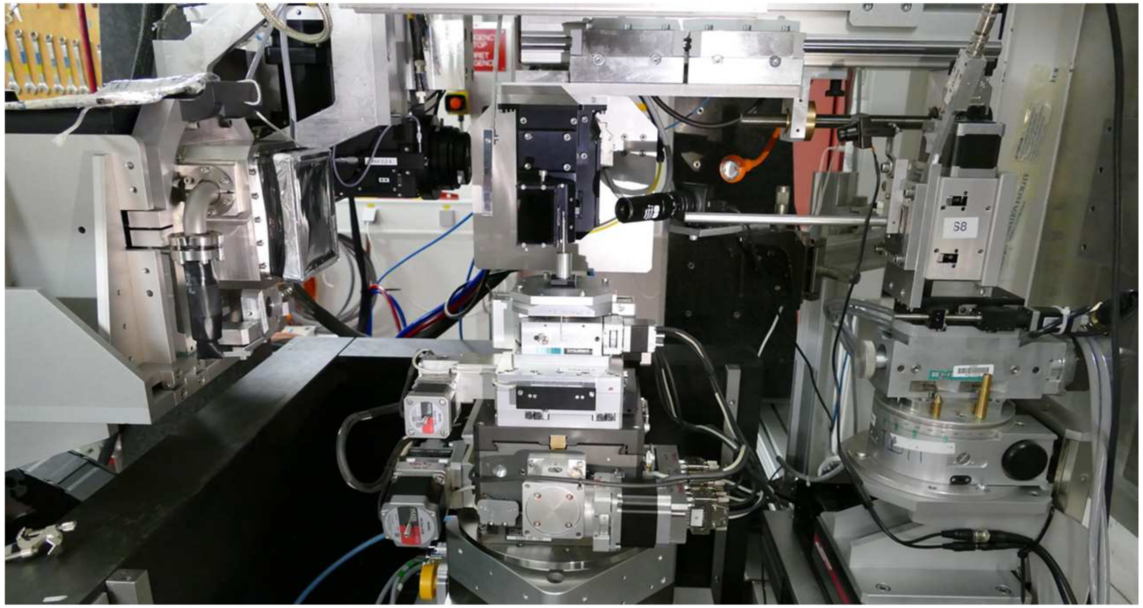

Diffraction based imaging at ID11, DCT and 3DXRD, near or far field ?

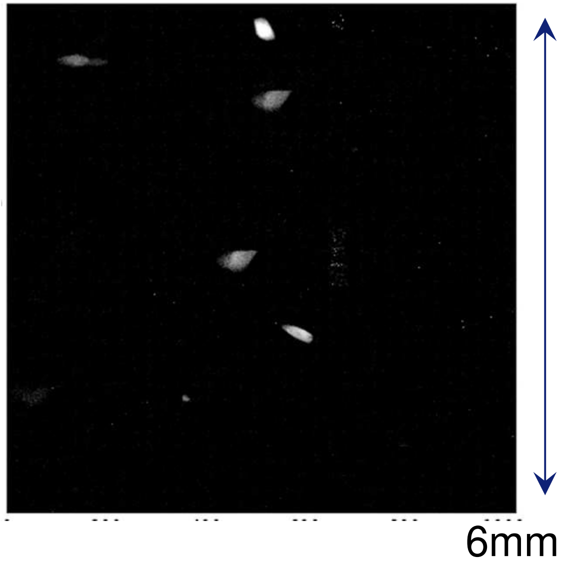

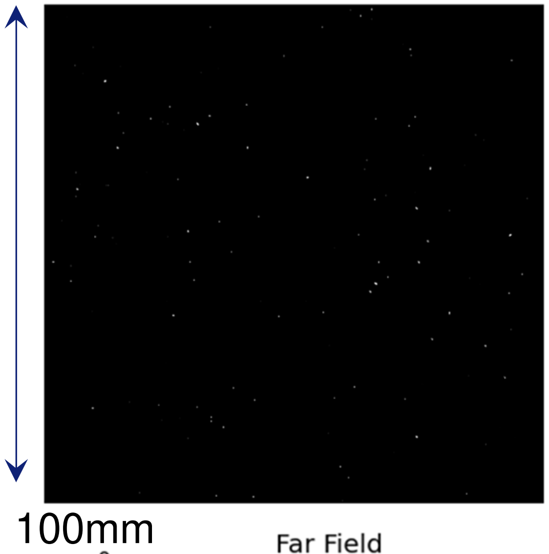

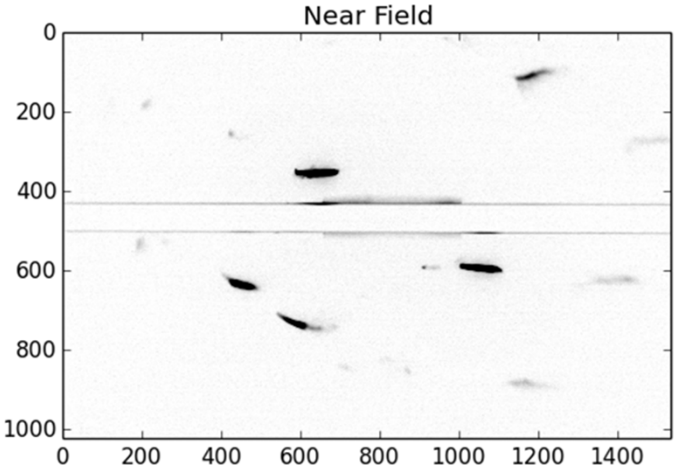

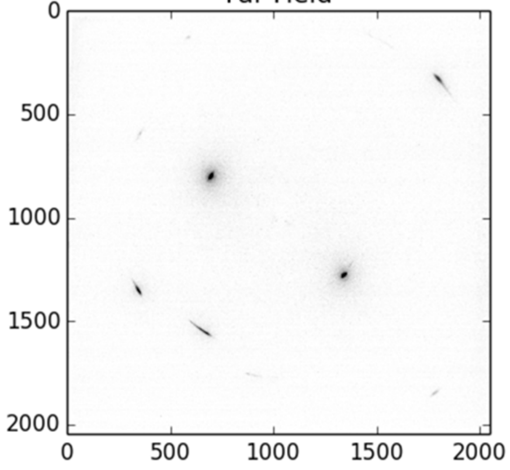

Majkut *et al*. J Am Ceram Soc 2016; 100: 393–402

Near field grain map for the same sample

Thermal annealing strains

Electrically poled

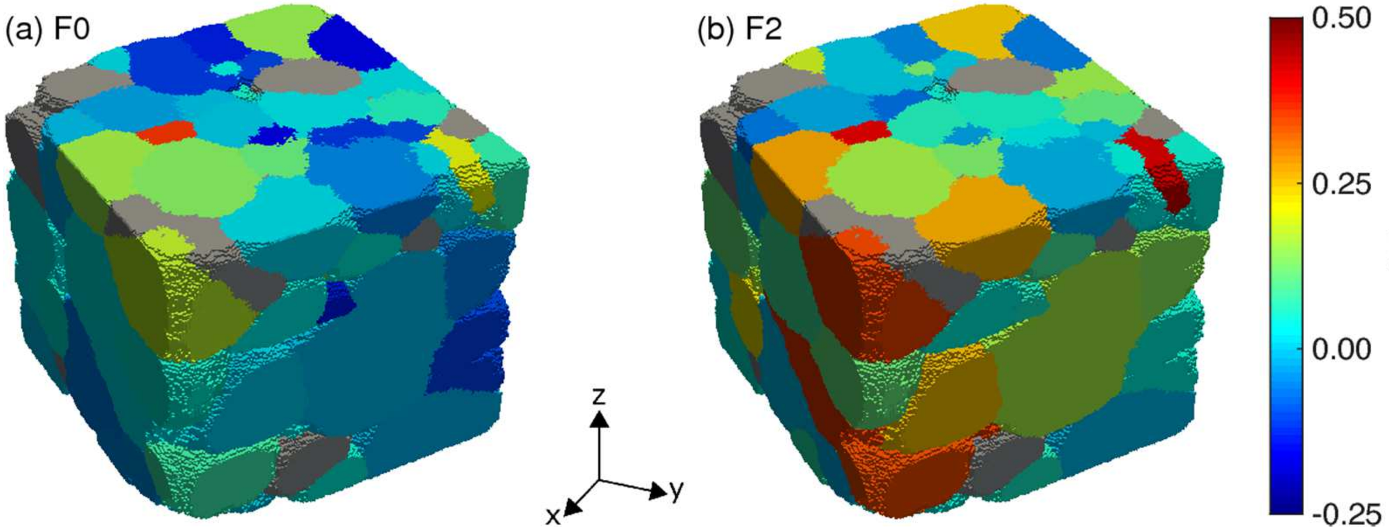

Three-dimensional full-field X-ray orientation microscopy

Nicola Viganò, Alexandre Tanguy, Simon Hallais, Alexandre Dimanov, Michel Bornert, Kees Joost Batenburg & Wolfgang Ludwig

Scientific Reports **6**, Article number: 20618 | Received: 25 September 2015

Figure 1: Comparison of EBSD surface mapping with the different reconstruction approaches for full-field X-ray orientation microscopy discussed in this work.

From: Three-dimensional full-field X-ray orientation microscopy

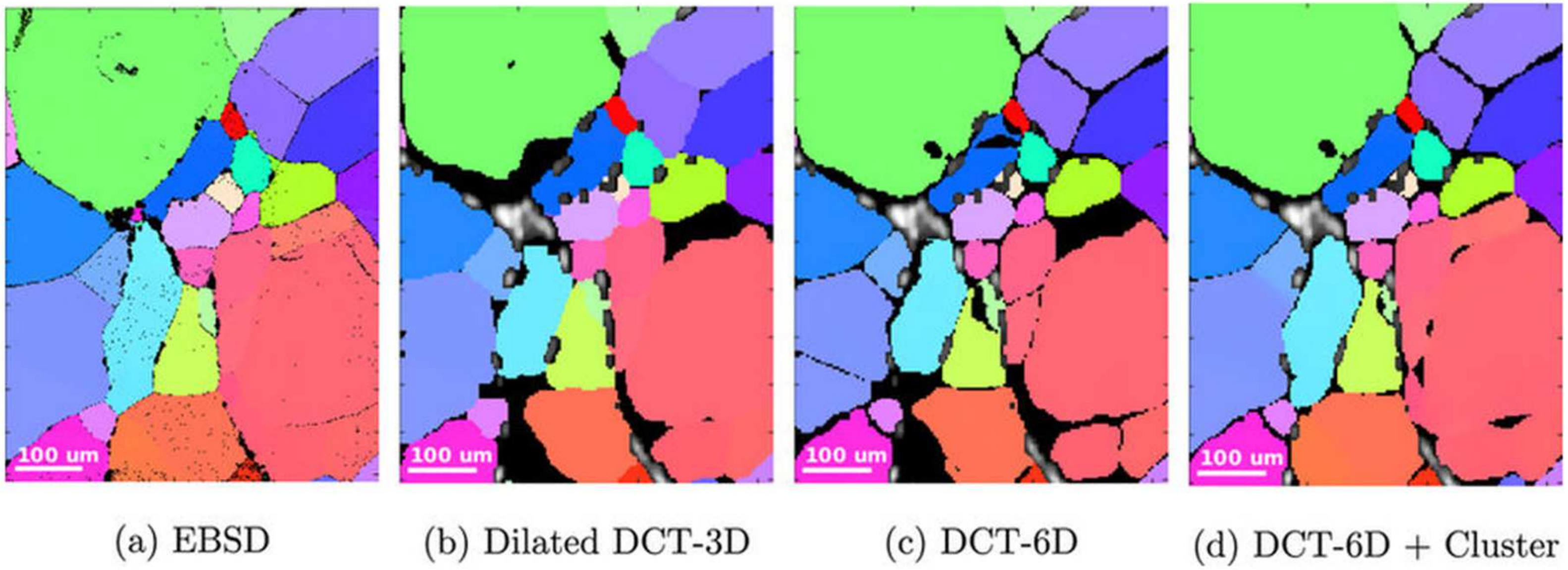

(a) EBSD (b) Dilated DCT-3D (c) DCT-6D (d) DCT-6D + Cluster

Mapping deformed grains

Vigano and Ludwig

Figure 2: Comparison of the experimental images for an [2 2 2] reflection at $\theta = 6.21$ *degrees*, $\eta = 112$ *degrees*, with a $\Delta\omega = 6.7$ *degrees* (67 images), with the same forward-projected spot from the result of the reconstruction.

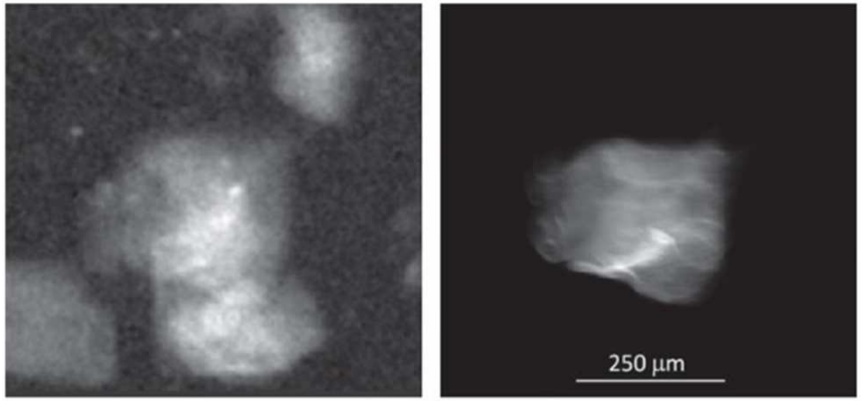

(a) Experimental spot image (b) Theoretically fwd-projected image

Figure 3: Reconstruction of a grain cluster using the extended 6D approach.

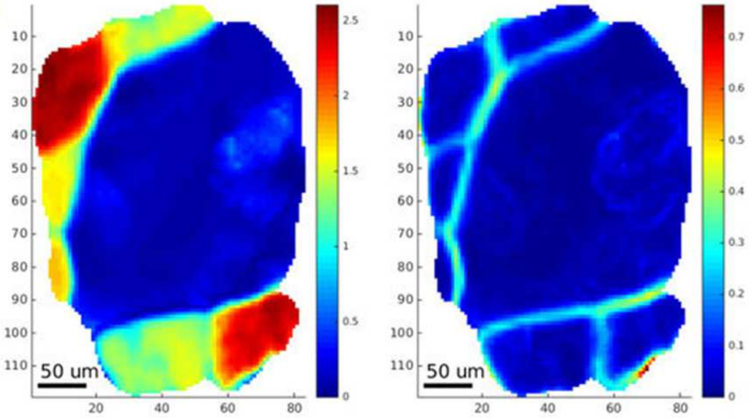

(a) Slice IGM (b) Slice KAM

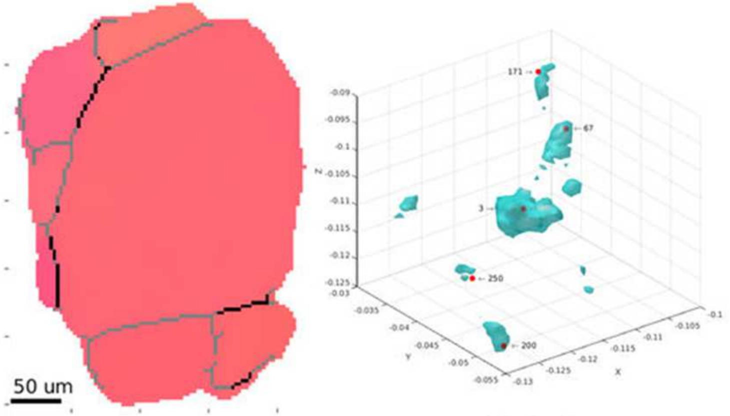

(c) IPF (d) ODF

(**a**–**c**) same slice through the 3D reconstruction showing: (**a**) Intra-granular Misorientation, (**b**) Kernel Average Misorientation (**c**) inverse pole figure colour coding scheme revealing the presence of sub-grains and small angle boundaries from skeletonization of (**a**) (gray: ≥0.5°, black: ≥2°), (**d**) iso-surface of the orientation sub-space reconstructed for the clustered region. Red points indicate sub-grain orientations which had been successfully identified

Force chains in granular matter

Combine 3D tomography : particle shapes and contacts
… with 3DXRD : particle strains (via crystal unit cells)

EPJ Web of Conferences **140**, 02006 (2017) DOI: 10.1051/epjconf/201714002006
Powders & Grains 2017

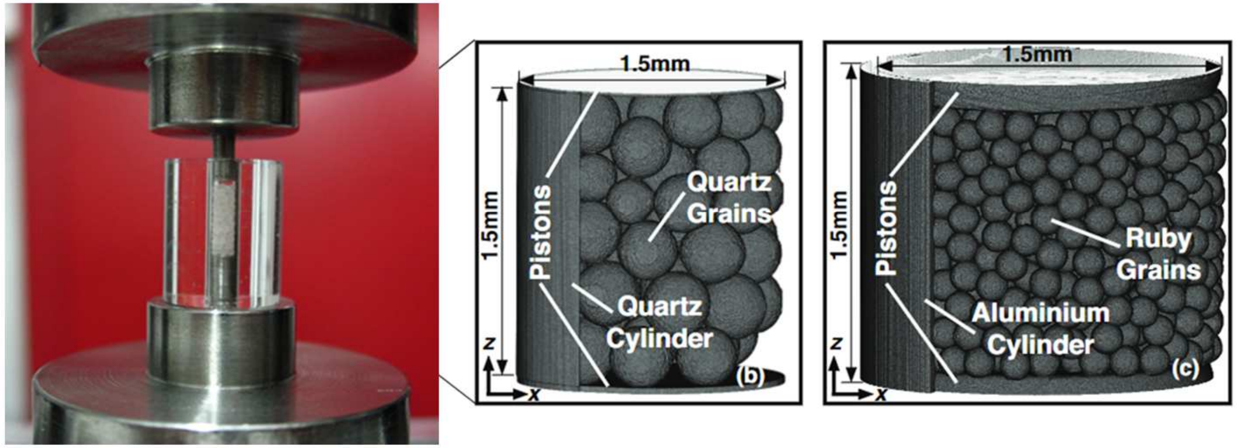

Figure 1. (a) Custom-built loading device positioned in beam line ID11 at ESRF, showing orientation of incident X-ray beam, rotation direction, and laboratory coordinate frame. (b) XRCT image of 77 single-crystal quartz grains in an amorphous quartz cylinder (also reported in [9]). (c) XRCT image of 1099 single-crystal ruby grains in an aluminium cylinder.

Compare to 2D photo-elastic experiments

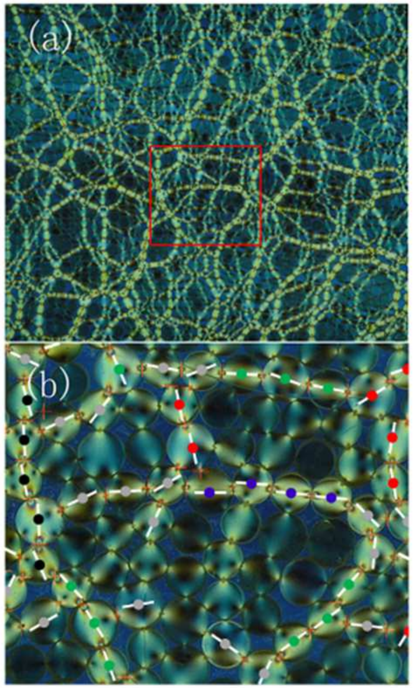

FIG. 2. (Color online) (a) An example of a force-chain network in a 2D layer of granular materials under isotropic compression. Here bidisperse photoelastic disks are used. (b) The portion of panel (a) indicated by the red rectangle, showing several force chains of different lengths using different colors. For example, chains of different lengths are displayed by painting each particle center using dots of different colors: black for length five, blue for length four, green for length three, and red for length two. The short line drawn on top of each particle represents the orientation of the force moment tensor of each particle. Particles with gray-dot centers do not belong to any force chain although satisfying $\sigma_1 \geqslant \langle\sigma_1\rangle$ (see Sec. II for details).

Force-chain distributions in granular systems
Phys. Rev. E **89**, 012203 (2014)
Ling Zhang, Yujie Wang, and Jie Zhang

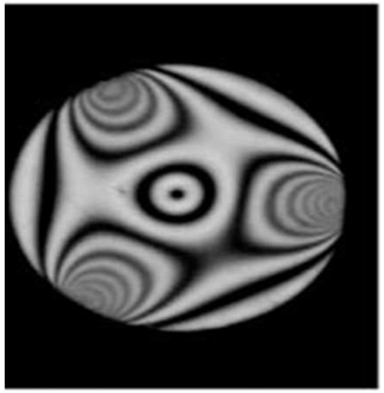

Nature **435**, 1079-1082 (2005)
Contact force measurements and stress-induced anisotropy in granular materials
T. S. Majmudar & R. P. Behringer

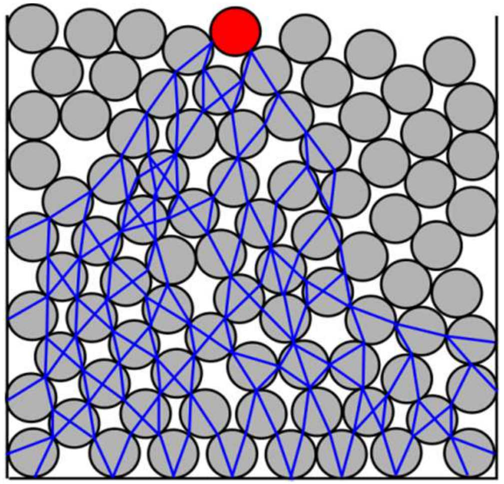

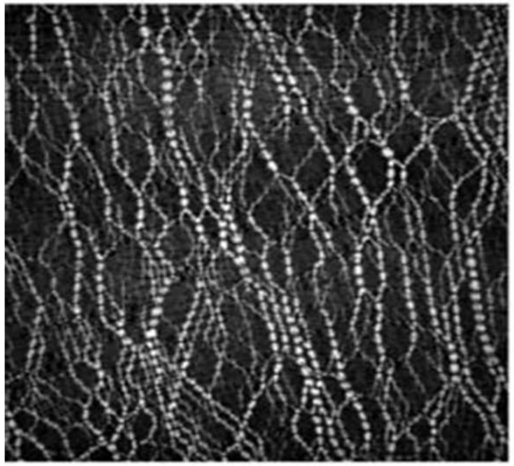

Natural sand grains

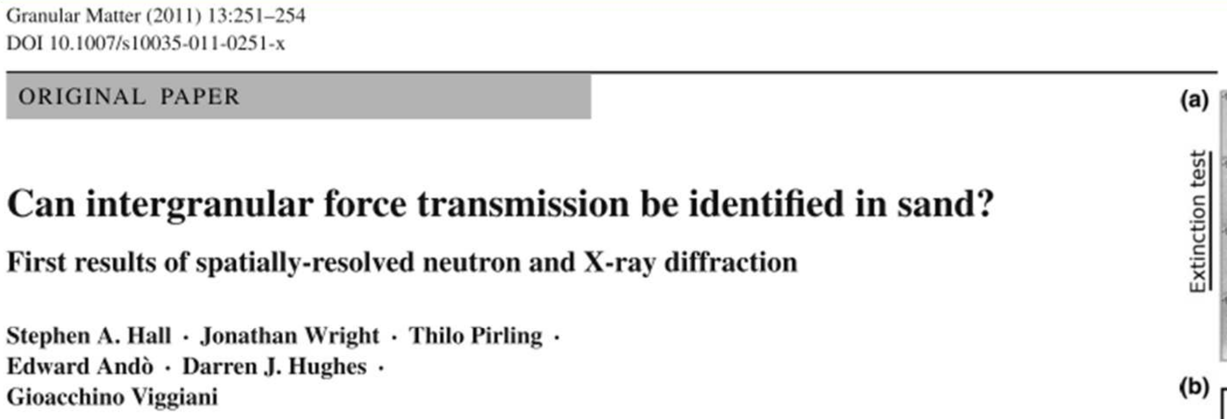

Granular Matter (2011) 13:251–254
DOI 10.1007/s10035-011-0251-x

ORIGINAL PAPER

Can intergranular force transmission be identified in sand?

First results of spatially-resolved neutron and X-ray diffraction

Stephen A. Hall · Jonathan Wright · Thilo Pirling ·
Edward Andò · Darren J. Hughes ·
Gioacchino Viggiani

Promising results but the natural sand grains showed significant internal structures (twins and cracks). On loading the internal domains move with respect to each other.

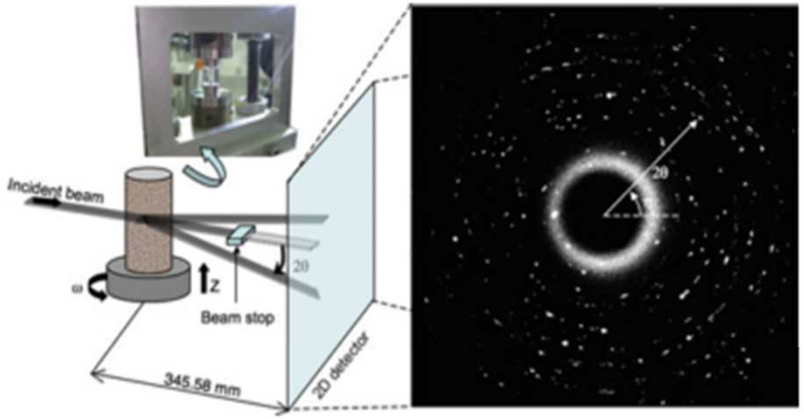

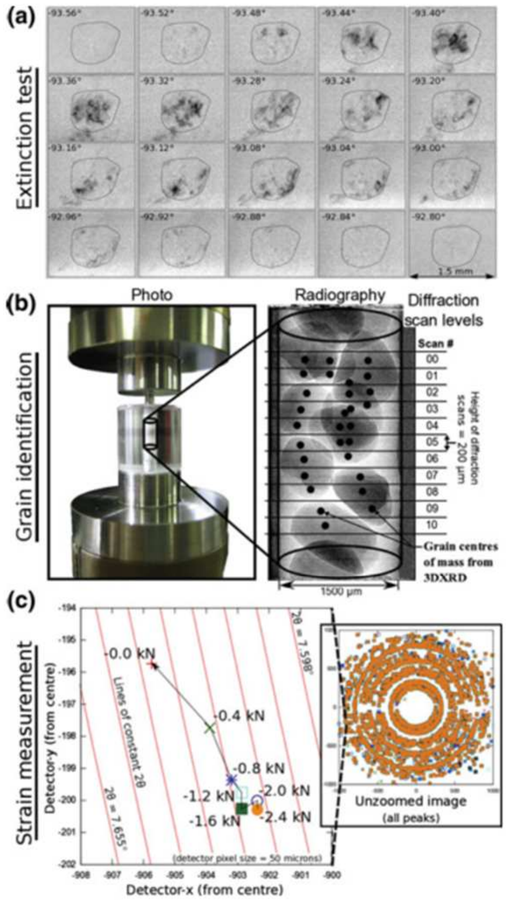

Larger system – Collaboration with Steve Hall, Ryan Hurley, Jose Andrade

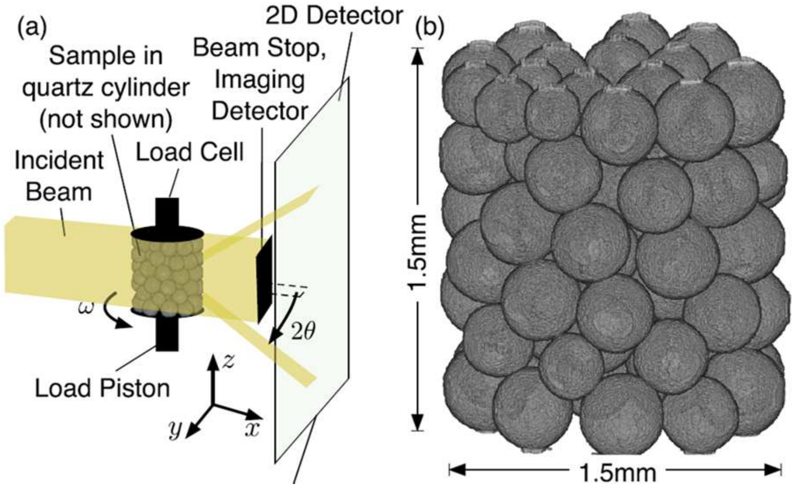

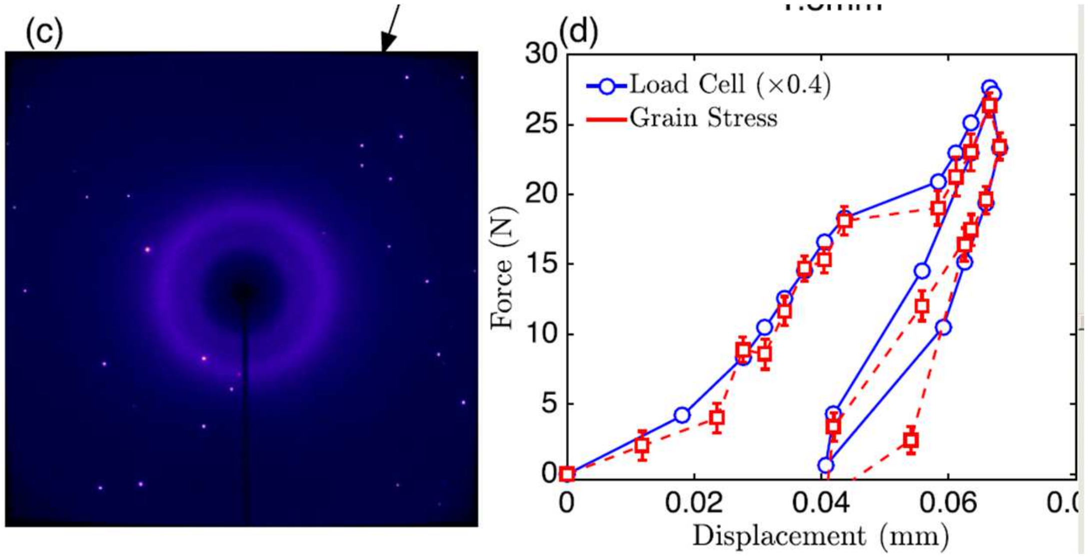

Analysis of strain tensors

Solve inversion problem

Determined contact forces

Strain tensors of the quartz grains versus applied load.

Quantitative mechanical force
Information

Color represents strain tensors
Mapped onto surface of grains

32 grains.

Geotechnique Letters ***5*** *236 2015*

3D EXPERIMENTAL GRANULAR MECHANICS

Stephen A. Hall

Division of Solid Mechanics, Lund University, Lund, Sweden & European Spallation Source AB, Lund, Sweden , stephen.hall@solid.lth.se

Jonathan Wright

European Synchrotron Radiation Facility, Grenoble, France, wright@esrf.fr

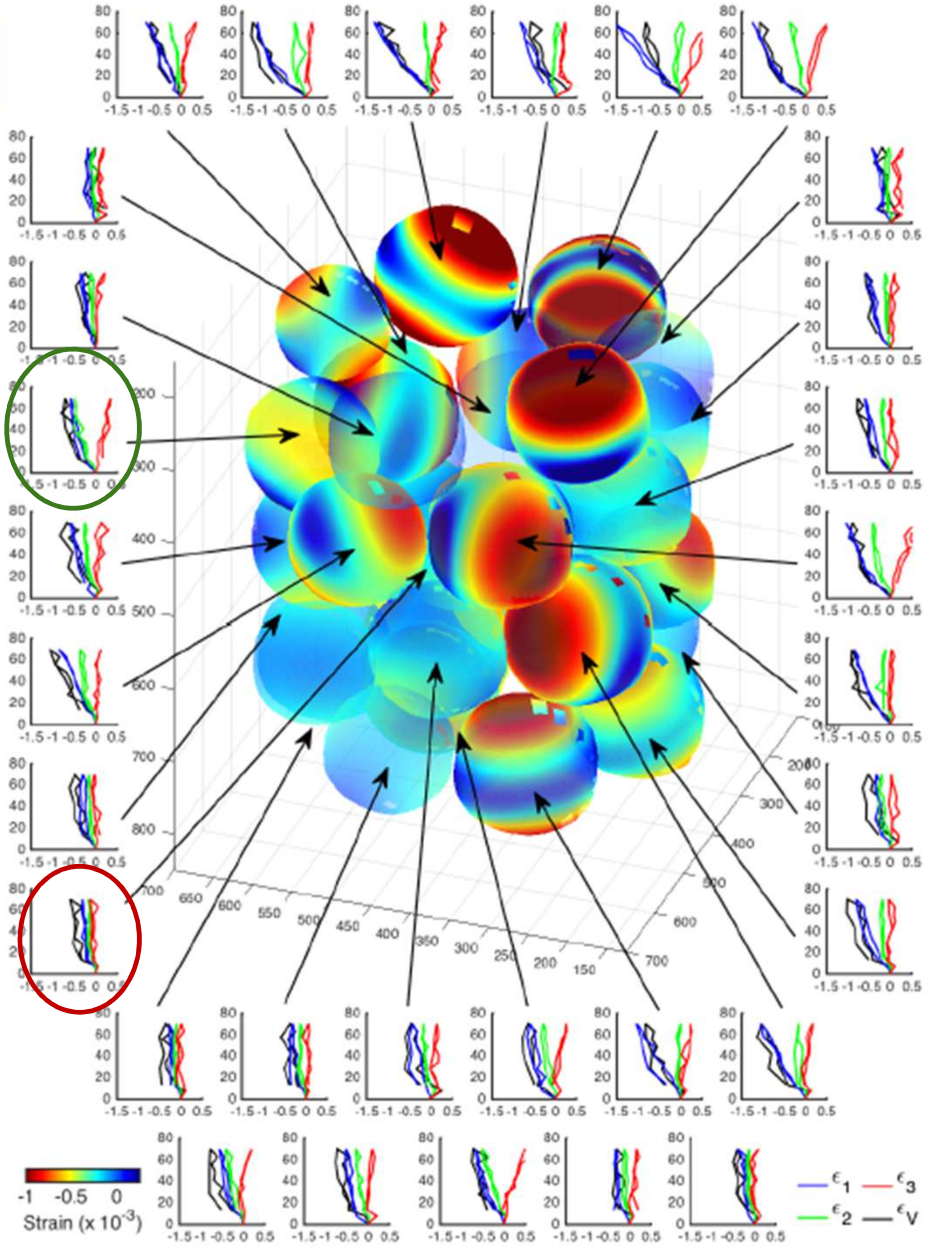

Synthetic quartz spheres

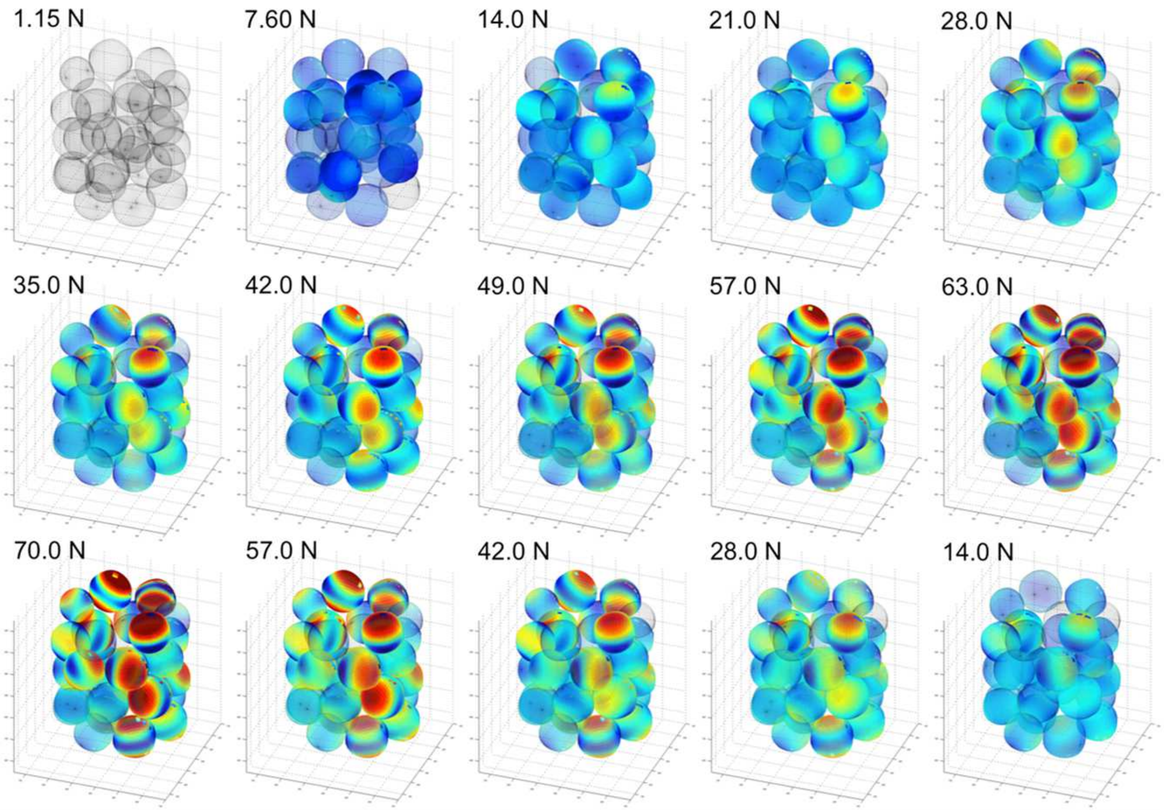

By polishing synthetic quartz spheres the internal structures could removed to give clean data. Images show the surfaces of the spheres found from tomography colored according to their strain tensors. Force chains are clearly evident.

Steve Hall, Lund

Mapping strains in shape memory alloy

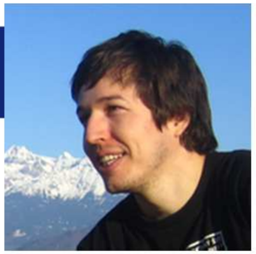

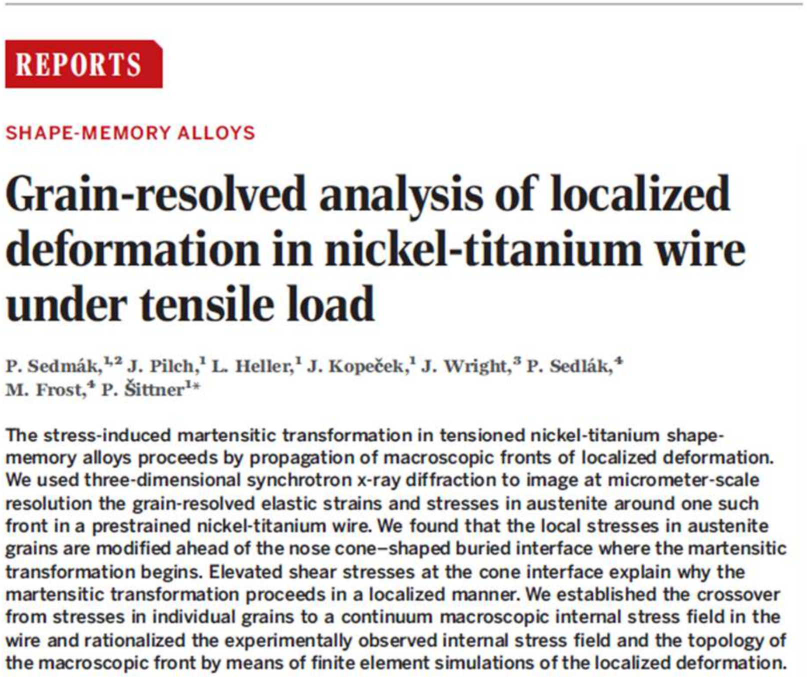

REPORTS

SHAPE-MEMORY ALLOYS

Grain-resolved analysis of localized deformation in nickel-titanium wire under tensile load

P. Sedmák,[1,2] J. Pilch,[1] L. Heller,[1] J. Kopeček,[1] J. Wright,[3] P. Sedlák,[4]
M. Frost,[4] P. Šittner[1*]

The stress-induced martensitic transformation in tensioned nickel-titanium shape-memory alloys proceeds by propagation of macroscopic fronts of localized deformation. We used three-dimensional synchrotron x-ray diffraction to image at micrometer-scale resolution the grain-resolved elastic strains and stresses in austenite around one such front in a prestrained nickel-titanium wire. We found that the local stresses in austenite grains are modified ahead of the nose cone–shaped buried interface where the martensitic transformation begins. Elevated shear stresses at the cone interface explain why the martensitic transformation proceeds in a localized manner. We established the crossover from stresses in individual grains to a continuum macroscopic internal stress field in the wire and rationalized the experimentally observed internal stress field and the topology of the macroscopic front by means of finite element simulations of the localized deformation.

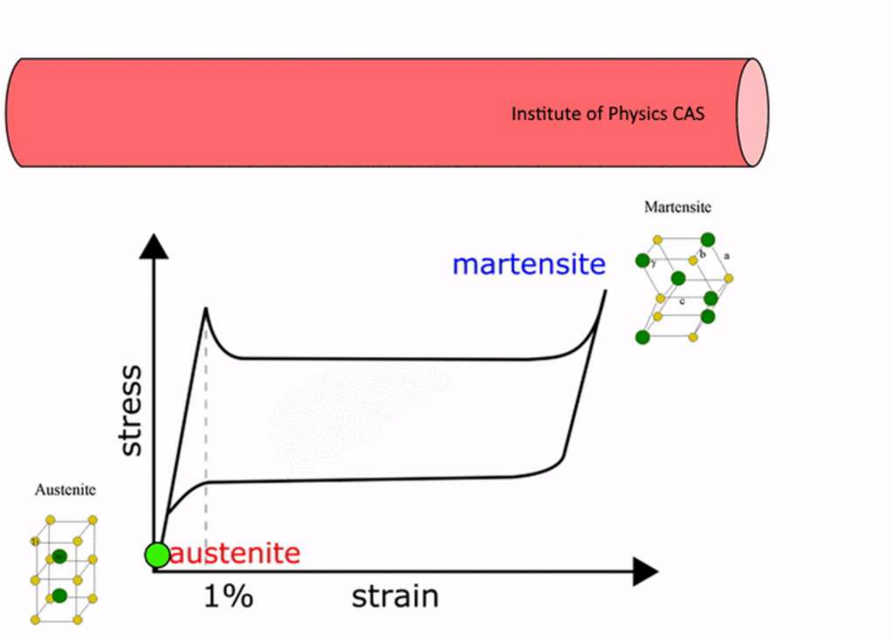

Science (2016) **353** 6299

NiTi Shape Memory Alloy

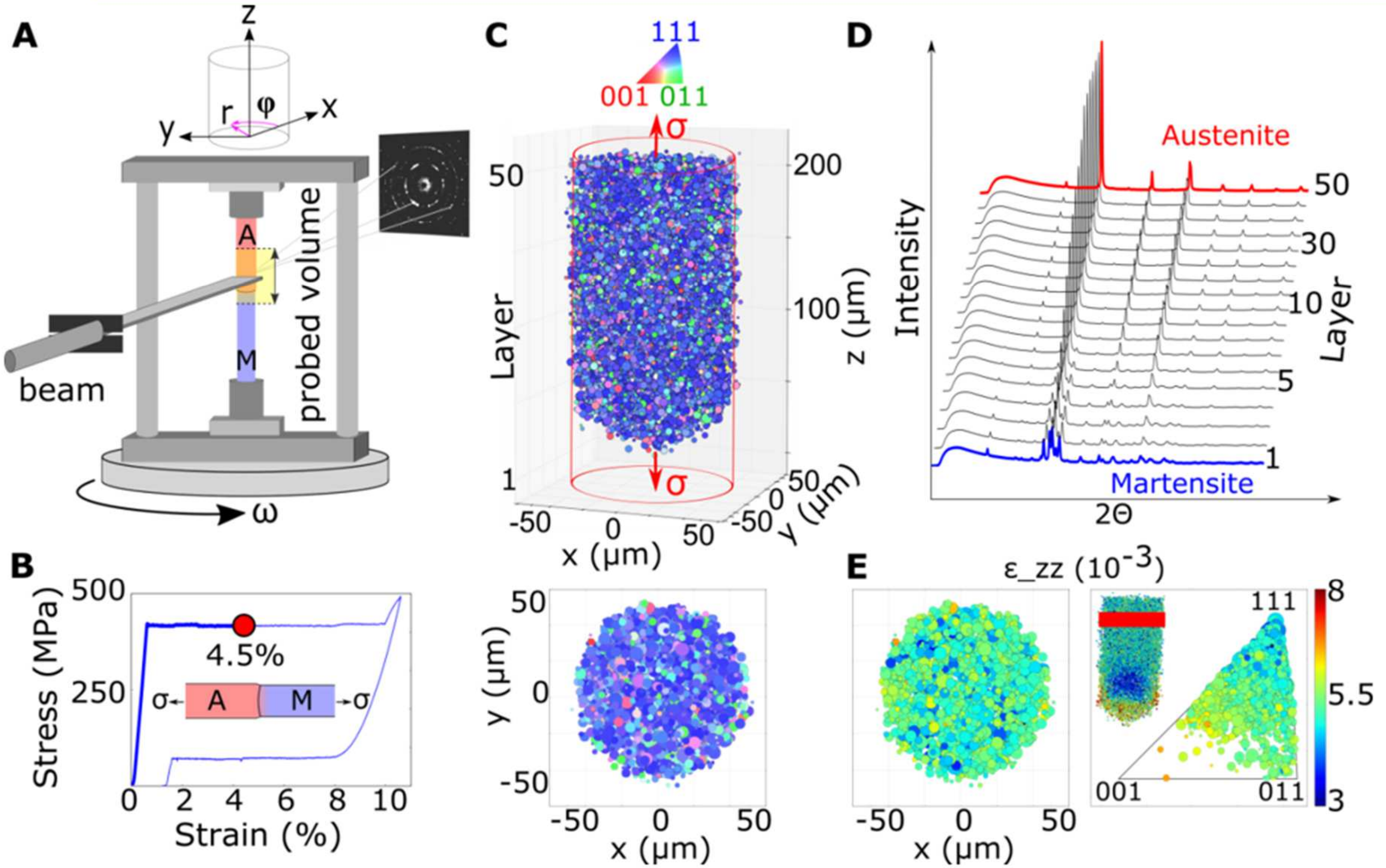

3D strain tensors at the martensite band front

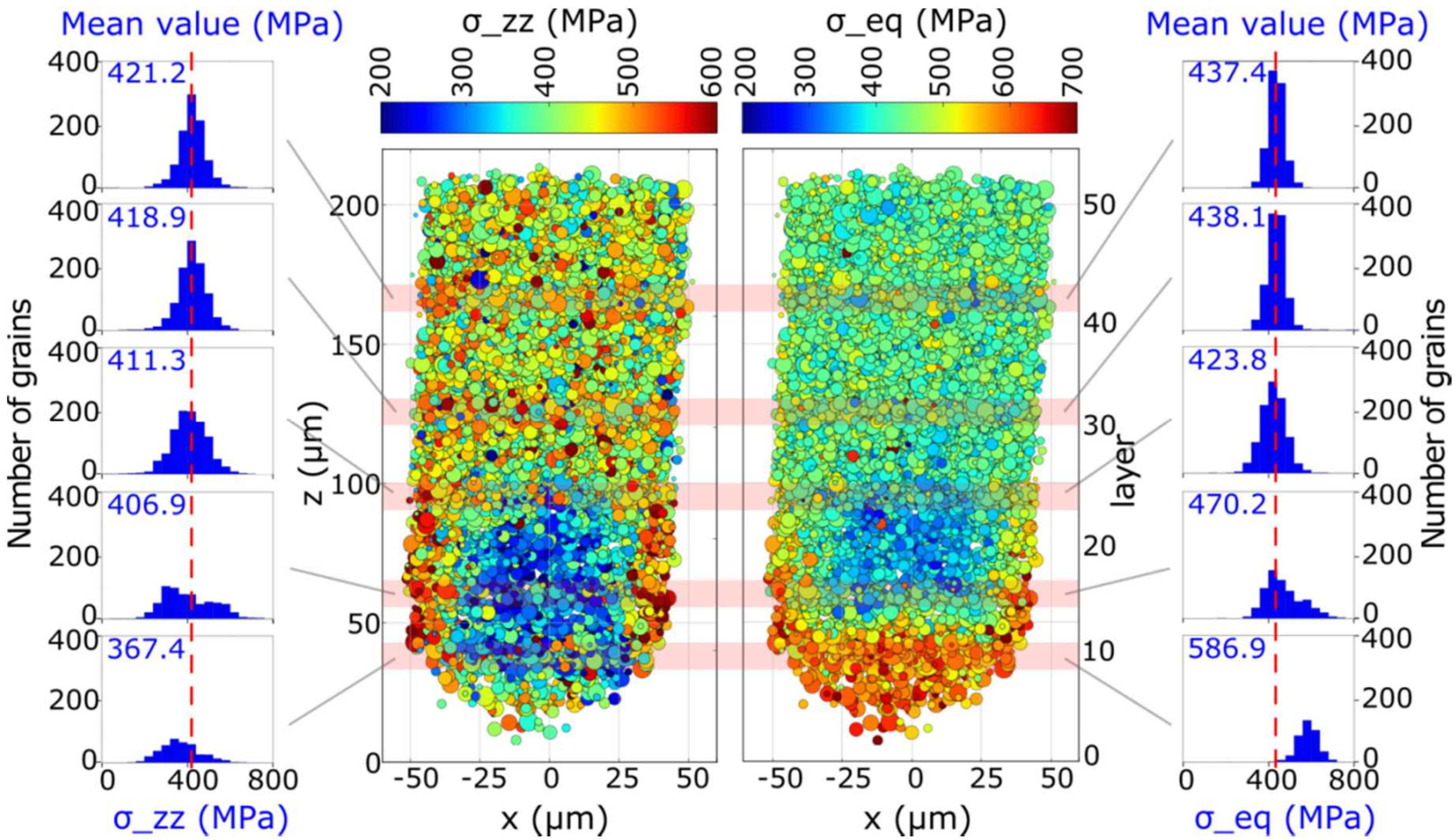

TEDDI
Tomographic Energy Dispersive Diffractive Imaging

µ-Laue
Micro Laue (Diffraction Mapping)

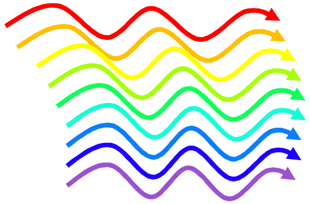

Polychromatic

DCT
Diffraction Constrast Tomography

3DXRD
3D X-ray diffraction

HEDM
High Energy Diffraction Microscopy

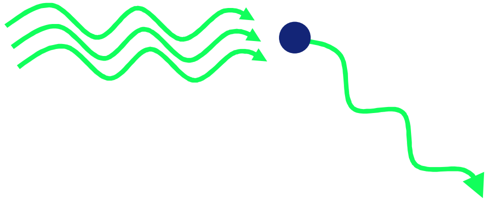

Monochromatic

XRDCT
X-ray Diffraction CT

XDT
X-ray Diffraction Tomography

PDFCT
Pair distribution function CT

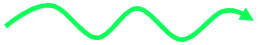

Scanning a smaller beam

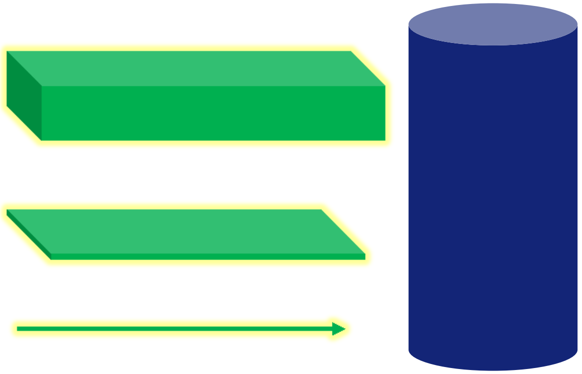

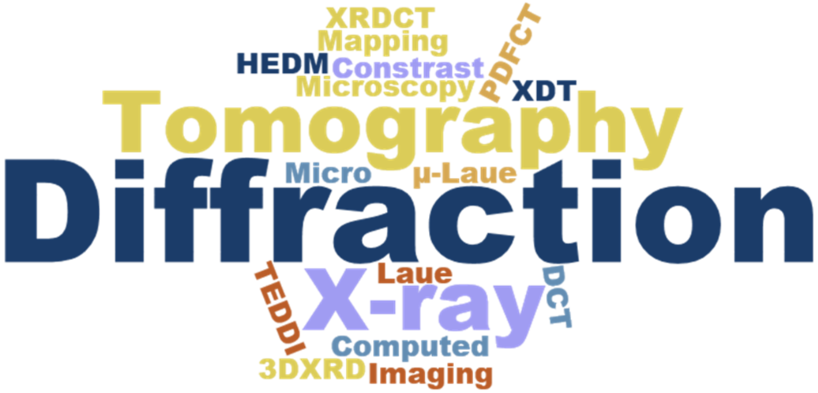

Tomography : how does it work ?

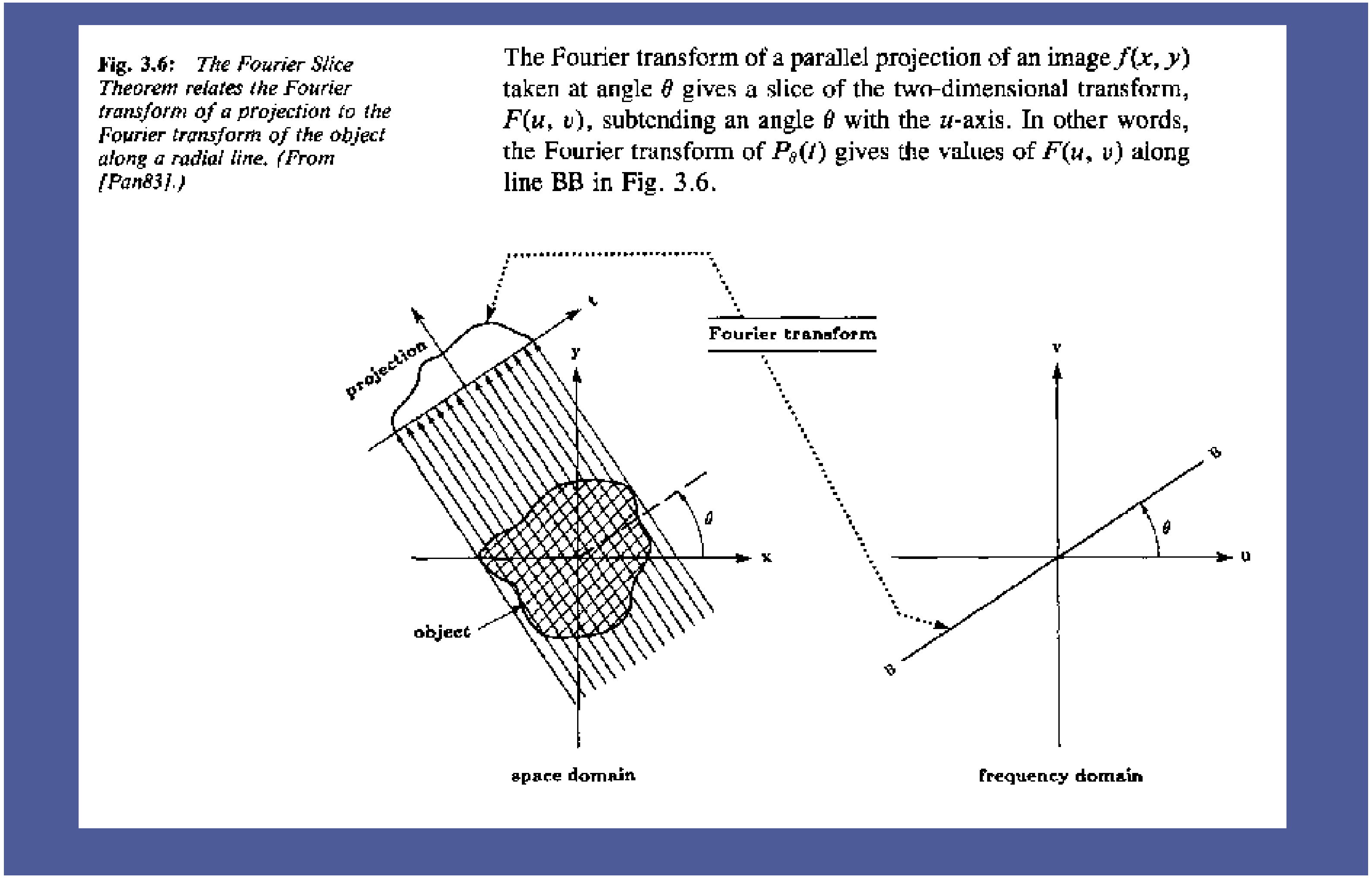

Fig. 3.6: *The Fourier Slice Theorem relates the Fourier transform of a projection to the Fourier transform of the object along a radial line. (From [Pan83].)*

The Fourier transform of a parallel projection of an image $f(x, y)$ taken at angle θ gives a slice of the two-dimensional transform, $F(u, v)$, subtending an angle θ with the u-axis. In other words, the Fourier transform of $P_\theta(t)$ gives the values of $F(u, v)$ along line BB in Fig. 3.6.

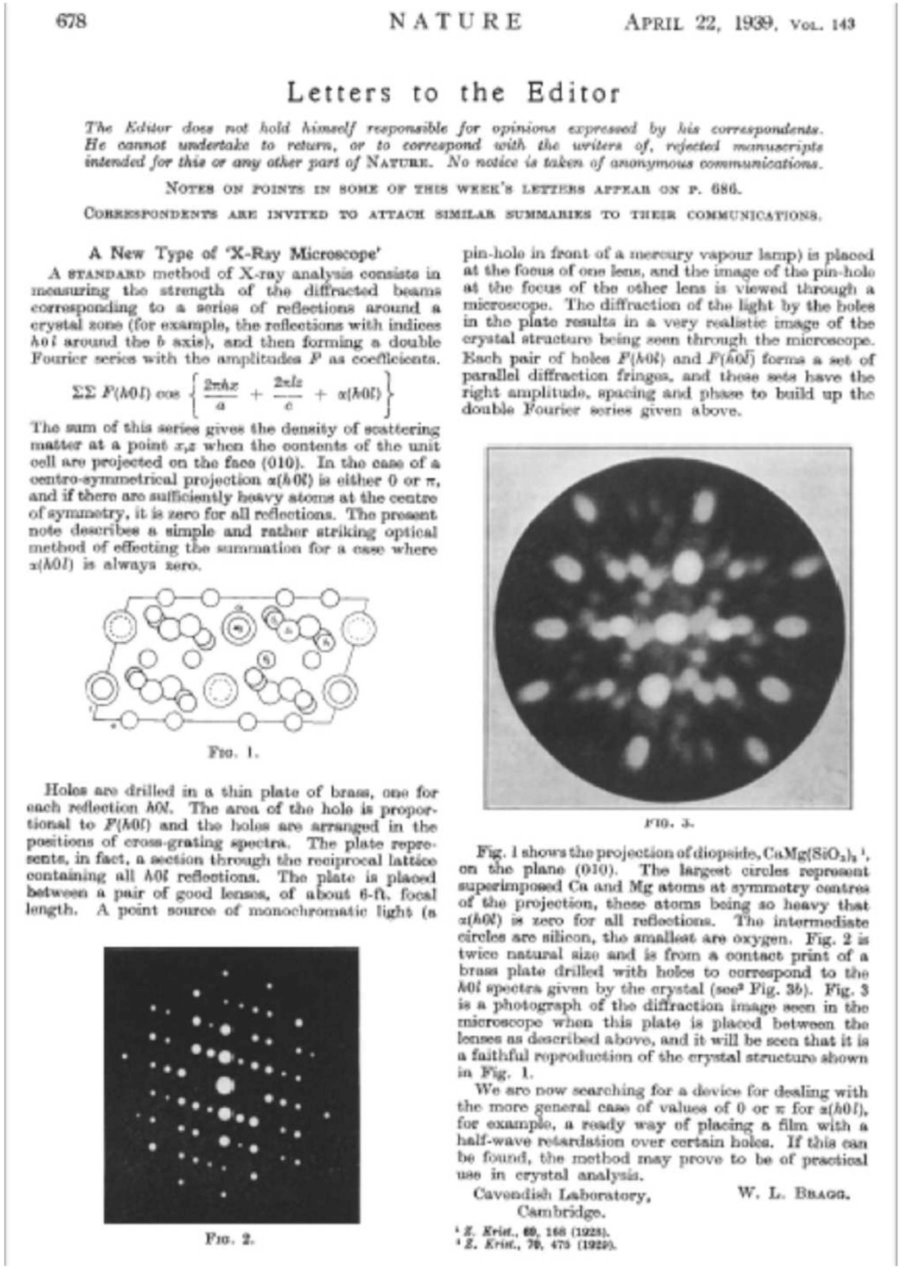

678 NATURE APRIL 22, 1939, VOL. 143

Letters to the Editor

The Editor does not hold himself responsible for opinions expressed by his correspondents. He cannot undertake to return, or to correspond with the writers of, rejected manuscripts intended for this or any other part of NATURE. *No notice is taken of anonymous communications.*

NOTES ON POINTS IN SOME OF THIS WEEK'S LETTERS APPEAR ON P. 686.

CORRESPONDENTS ARE INVITED TO ATTACH SIMILAR SUMMARIES TO THEIR COMMUNICATIONS.

A New Type of 'X-Ray Microscope'

A STANDARD method of X-ray analysis consists in measuring the strength of the diffracted beams corresponding to a series of reflections around a crystal zone (for example, the reflections with indices $h0l$ around the b axis), and then forming a double Fourier series with the amplitudes F as coefficients.

$$\Sigma\Sigma\ F(h0l)\cos\left\{\frac{2\pi hx}{a}+\frac{2\pi lz}{c}+\alpha(h0l)\right\}$$

The sum of this series gives the density of scattering matter at a point x,z when the contents of the unit cell are projected on the face (010). In the case of a centro-symmetrical projection $\alpha(h0l)$ is either 0 or π, and if there are sufficiently heavy atoms at the centre of symmetry, it is zero for all reflections. The present note describes a simple and rather striking optical method of effecting the summation for a case where $\alpha(h0l)$ is always zero.

FIG. 1.

Holes are drilled in a thin plate of brass, one for each reflection $h0l$. The area of the hole is proportional to $F(h0l)$ and the holes are arranged in the positions of cross-grating spectra. The plate represents, in fact, a section through the reciprocal lattice containing all $h0l$ reflections. The plate is placed between a pair of good lenses, of about 6-ft. focal length. A point source of monochromatic light (a pin-hole in front of a mercury vapour lamp) is placed at the focus of one lens, and the image of the pin-hole at the focus of the other lens is viewed through a microscope. The diffraction of the light by the holes in the plate results in a very realistic image of the crystal structure being seen through the microscope. Each pair of holes $F(h0l)$ and $F(\bar{h}0\bar{l})$ forms a set of parallel diffraction fringes, and these sets have the right amplitude, spacing and phase to build up the double Fourier series given above.

FIG. 2.

FIG. 3.

Fig. 1 shows the projection of diopside, $CaMg(SiO_3)_2$[1], on the plane (010). The largest circles represent superimposed Ca and Mg atoms at symmetry centres of the projection, these atoms being so heavy that $\alpha(h0l)$ is zero for all reflections. The intermediate circles are silicon, the smallest are oxygen. Fig. 2 is twice natural size and is from a contact print of a brass plate drilled with holes to correspond to the $h0l$ spectra given by the crystal (see[2] Fig. 3b). Fig. 3 is a photograph of the diffraction image seen in the microscope when this plate is placed between the lenses as described above, and it will be seen that it is a faithful reproduction of the crystal structure shown in Fig. 1.

We are now searching for a device for dealing with the more general case of values of 0 or π for $\alpha(h0l)$, for example, a ready way of placing a film with a half-wave retardation over certain holes. If this can be found, the method may prove to be of practical use in crystal analysis.

Cavendish Laboratory,
Cambridge.

W. L. BRAGG.

---

[1] *Z. Krist.*, 69, 168 (1928).

[2] *Z. Krist.*, 70, 475 (1929).

(h,0,l) : reflections give
Structure projection down b (or y)

…. etc = tomography

APRIL 22, 1939, VOL. 143

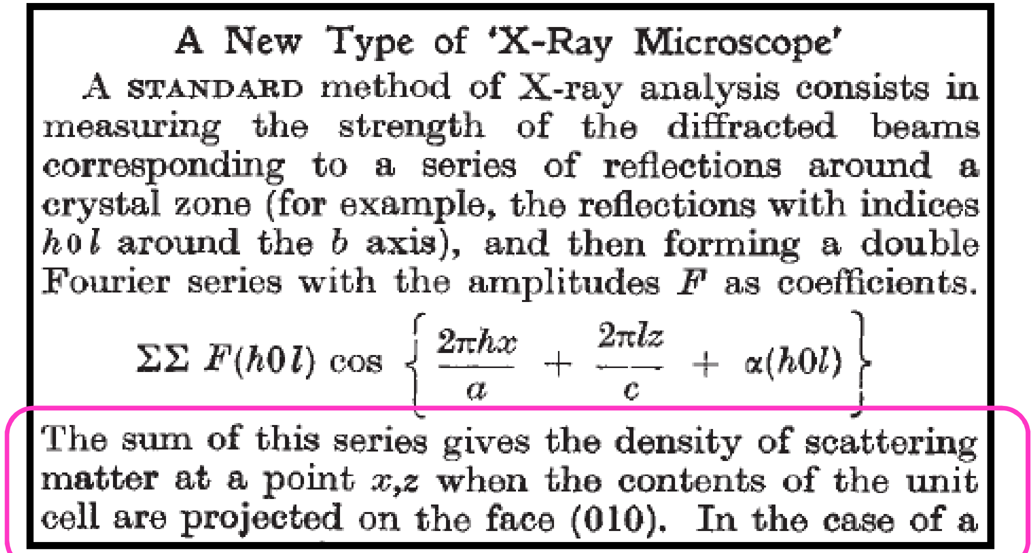

A New Type of 'X-Ray Microscope'

A STANDARD method of X-ray analysis consists in measuring the strength of the diffracted beams corresponding to a series of reflections around a crystal zone (for example, the reflections with indices $h0l$ around the b axis), and then forming a double Fourier series with the amplitudes F as coefficients.

$$\Sigma\Sigma\ F(h0l)\cos\left\{\frac{2\pi hx}{a}+\frac{2\pi lz}{c}+\alpha(h0l)\right\}$$

The sum of this series gives the density of scattering matter at a point x,z when the contents of the unit cell are projected on the face (010). In the case of a

Focus X-ray beam to adapt to sample…

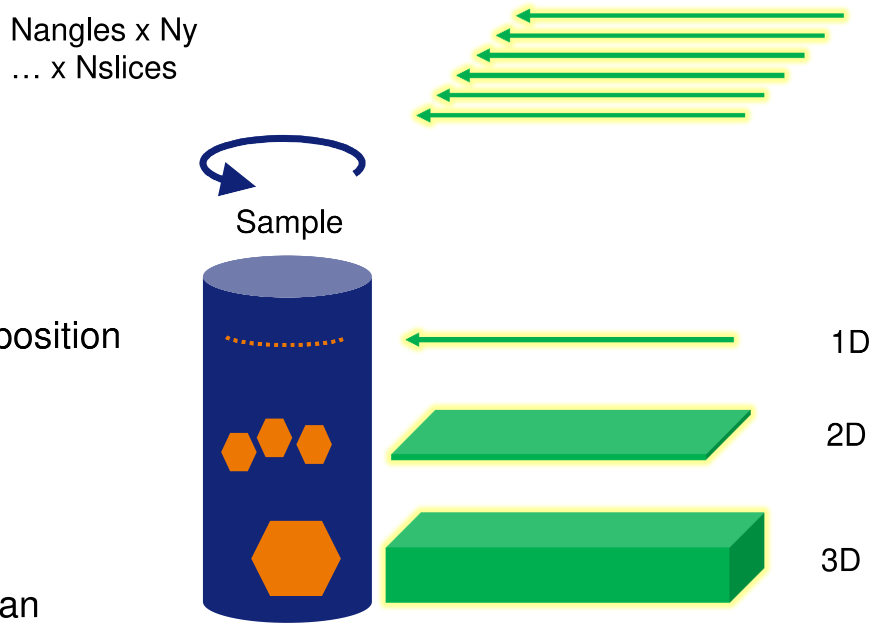

1D – Must scan rotation and sample position

2D – Measure a single slice,
need to stack many

3D – Measure a full volume in one scan

- Phase pure data from mixtures
- Single crystals from powders

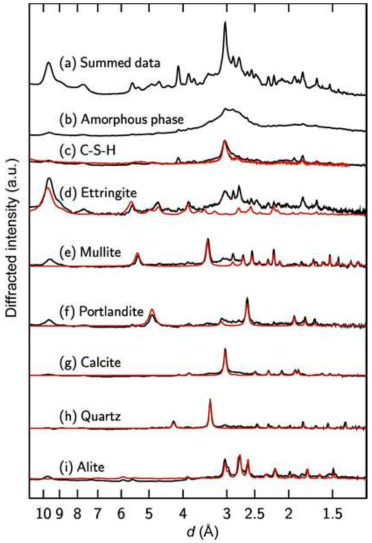

Cements: Phases separated

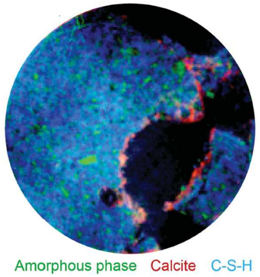

IUCrJ

Claret *et al.*

Volume 5 | **Part 2** | March 2018 | Pages 150–157 | 10.1107/S205225251701836X

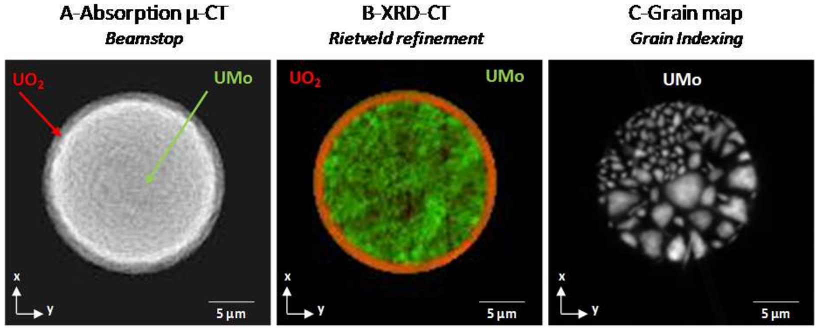

3DXRD: Crystals in powders

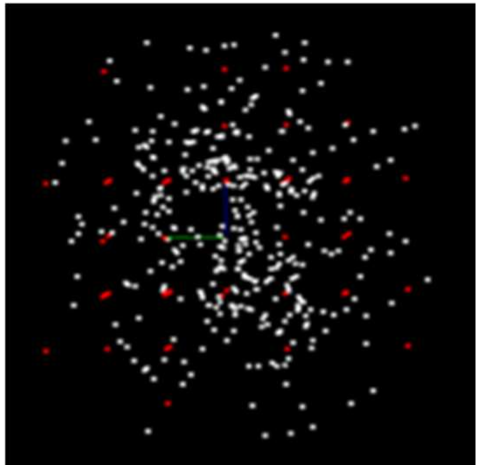

Filling the sinogram : data collection

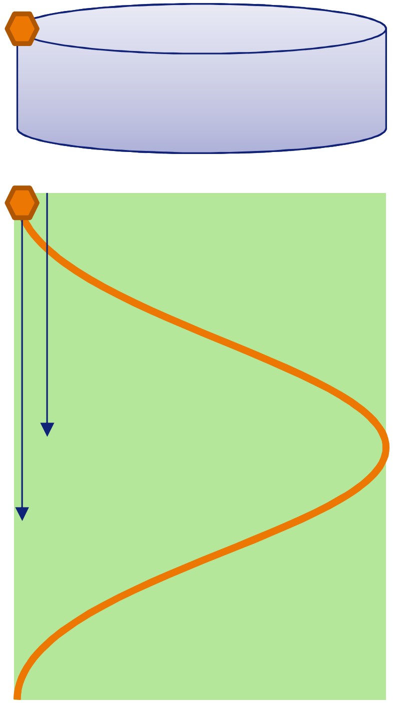

2D scans

Rotation angle
Position across sample

Stack layers for 3d

Deciphering mineralogical changes and carbonation development during hydration and ageing of a consolidated ternary blended cement paste

IUCrJ (2018). **5**, 150–157

Francis Claret,[a]* Sylvain Grangeon,[a] Annick Loschetter,[a] Christophe Tournassat,[a,b,c] Wout De Nolf,[d] Nicholas Harker,[d] Faiza Boulahya,[a] Stéphane Gaboreau,[a] Yannick Linard,[e] Xavier Bourbon,[e] Alejandro Fernandez-Martinez[f] and Jonathan Wright[d]

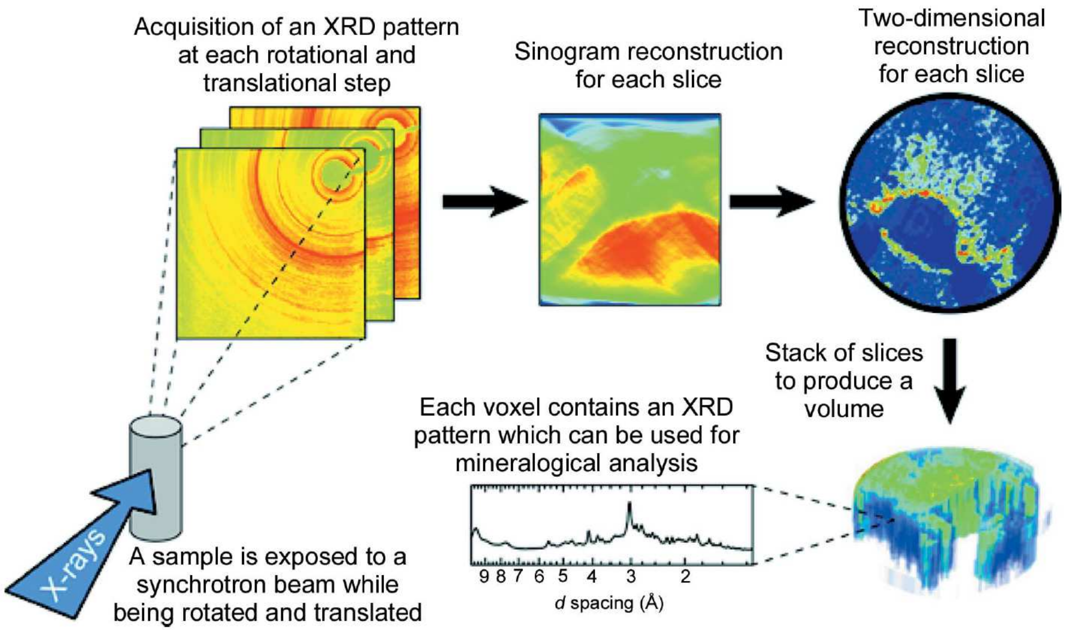

Acquisition of an XRD pattern at each rotational and translational step

Sinogram reconstruction for each slice

Two-dimensional reconstruction for each slice

Stack of slices to produce a volume

Each voxel contains an XRD pattern which can be used for mineralogical analysis

A sample is exposed to a synchrotron beam while being rotated and translated

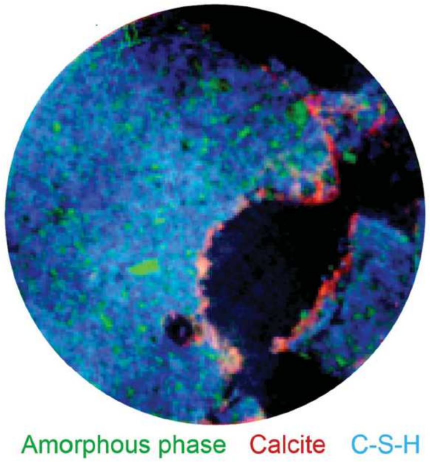

Claret *et-al* IUCrJ *2018*

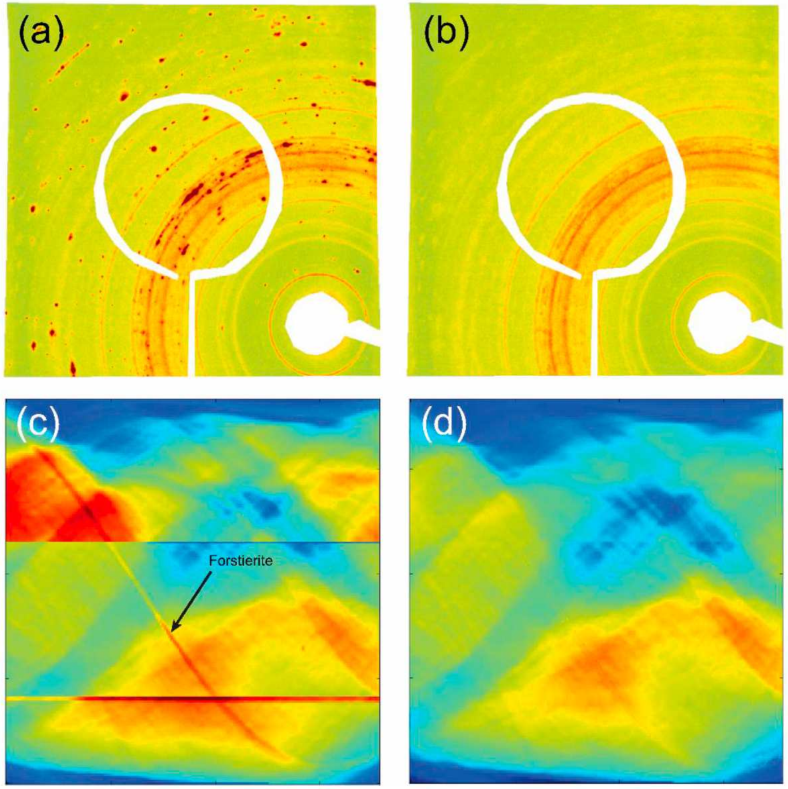

"Spotty" phases were **removed** by image processing. Ring-by-ring approach used to preserve textured powder lines

Data were also scaled/corrected for ring current decay

(See also Vamvakeros et al, JAC 2015, etc)

Claret *et al.*
IUCrJ **Volume 5** | **Part 2** | March 2018 | Pages 150–157 | 10.1107/S205225251701836X

Ever faster 2D detectors

1 second per picture	1 hour = 3600 seconds =	2D : 60 x 60 3D : 15 x 15 x 15
10 pictures per second	1 hour = 36000 frames =	2D : 180 x 180 3D : 33 x 33 x 33
100 fps	1 hour = 360000 frames =	2D : 600 x 600 3D : 71 x 71 x 71
500 fps (next year !)	1 hour = 1.8 Million frames =	2D : 1440x1250 3D : 122 x 122 x 122

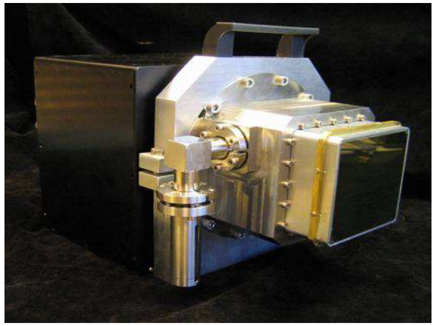

ESRF Frelon CCD

Pixel detectors

XRD-CT : Dorota Matras *et al*

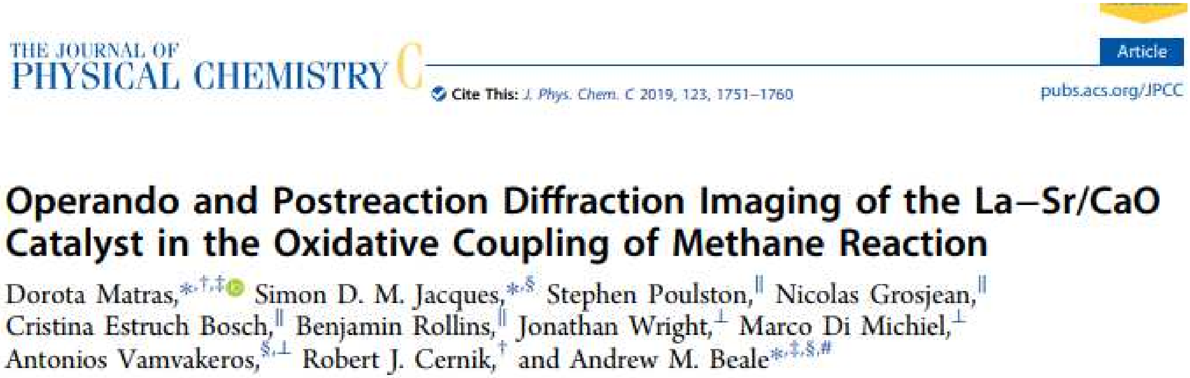

THE JOURNAL OF PHYSICAL CHEMISTRY C

Article

Cite This: J. Phys. Chem. C 2019, 123, 1751−1760

pubs.acs.org/JPCC

Operando and Postreaction Diffraction Imaging of the La−Sr/CaO Catalyst in the Oxidative Coupling of Methane Reaction

Dorota Matras,[*,†,‡] Simon D. M. Jacques,[*,§] Stephen Poulston,[‖] Nicolas Grosjean,[‖] Cristina Estruch Bosch,[‖] Benjamin Rollins,[‖] Jonathan Wright,[⊥] Marco Di Michiel,[⊥] Antonios Vamvakeros,[§,⊥] Robert J. Cernik,[†] and Andrew M. Beale[*,‡,§,#]

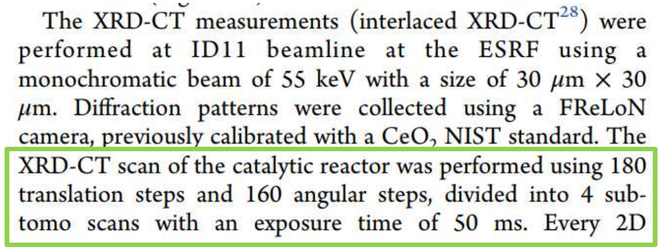

The XRD-CT measurements (interlaced XRD-CT[28]) were performed at ID11 beamline at the ESRF using a monochromatic beam of 55 keV with a size of 30 μm × 30 μm. Diffraction patterns were collected using a FReLoN camera, previously calibrated with a CeO_2 NIST standard. The XRD-CT scan of the catalytic reactor was performed using 180 translation steps and 160 angular steps, divided into 4 sub-tomo scans with an exposure time of 50 ms. Every 2D

2D (ID11) : 180 x 160 x 50 ms ~ 24 minutes

3D (ID15) : 100 x 100 x 36 x 20 ms ~ 2 hours

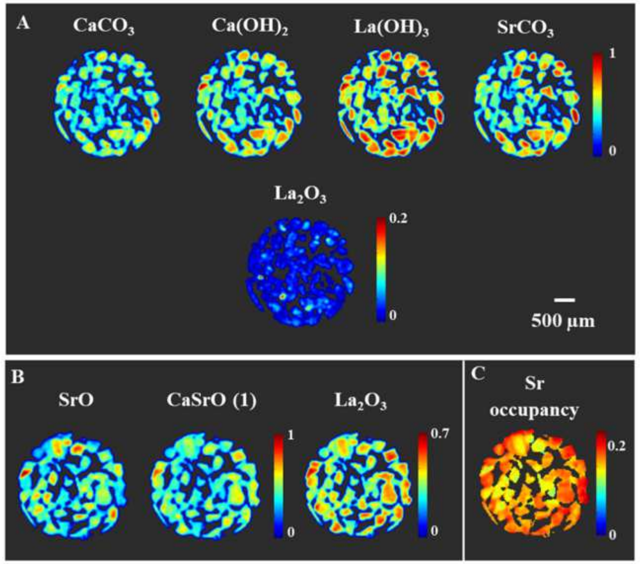

Figure 2. Spatial distribution of the La−Sr/CaO catalyst components at panel A: room temperature and panel B: at 780 °C in He. In the case of La_2O_3, the image was scaled to [0 0.2] for room temperature and [0 0.7] for 780 °C data for better visibility/contrast. Panel C: The spatial distribution occupancy of Sr in mixed CaO−SrO (1) oxide.

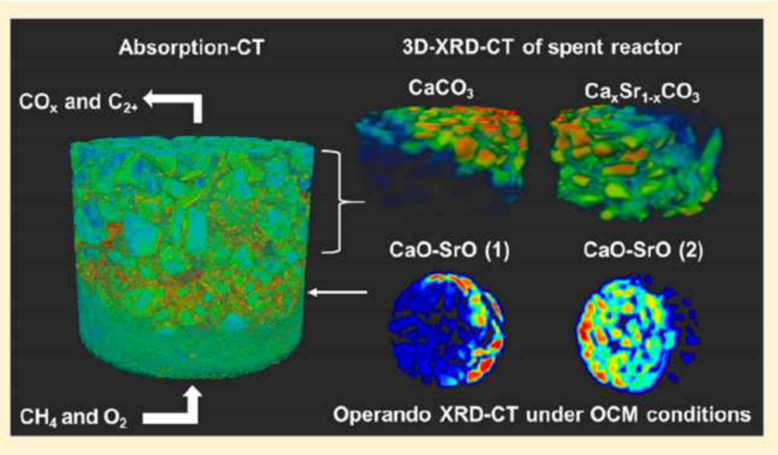

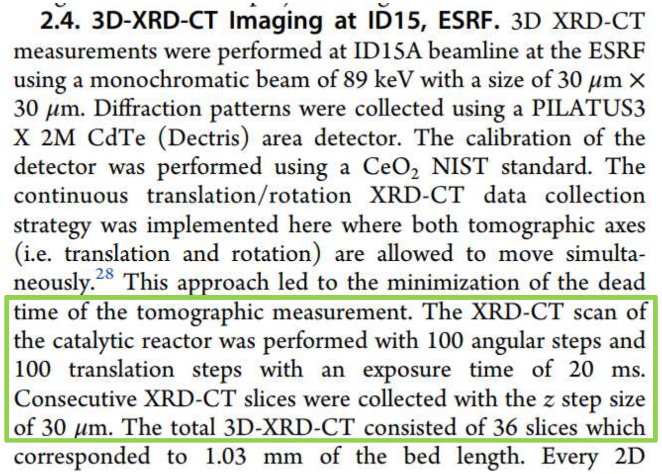

2.4. 3D-XRD-CT Imaging at ID15, ESRF. 3D XRD-CT measurements were performed at ID15A beamline at the ESRF using a monochromatic beam of 89 keV with a size of 30 μm × 30 μm. Diffraction patterns were collected using a PILATUS3 X 2M CdTe (Dectris) area detector. The calibration of the detector was performed using a CeO_2 NIST standard. The continuous translation/rotation XRD-CT data collection strategy was implemented here where both tomographic axes (i.e. translation and rotation) are allowed to move simultaneously.[28] This approach led to the minimization of the dead time of the tomographic measurement. The XRD-CT scan of the catalytic reactor was performed with 100 angular steps and 100 translation steps with an exposure time of 20 ms. Consecutive XRD-CT slices were collected with the z step size of 30 μm. The total 3D-XRD-CT consisted of 36 slices which corresponded to 1.03 mm of the bed length. Every 2D

Scanning 3DXRD - Select frames / spots on green line

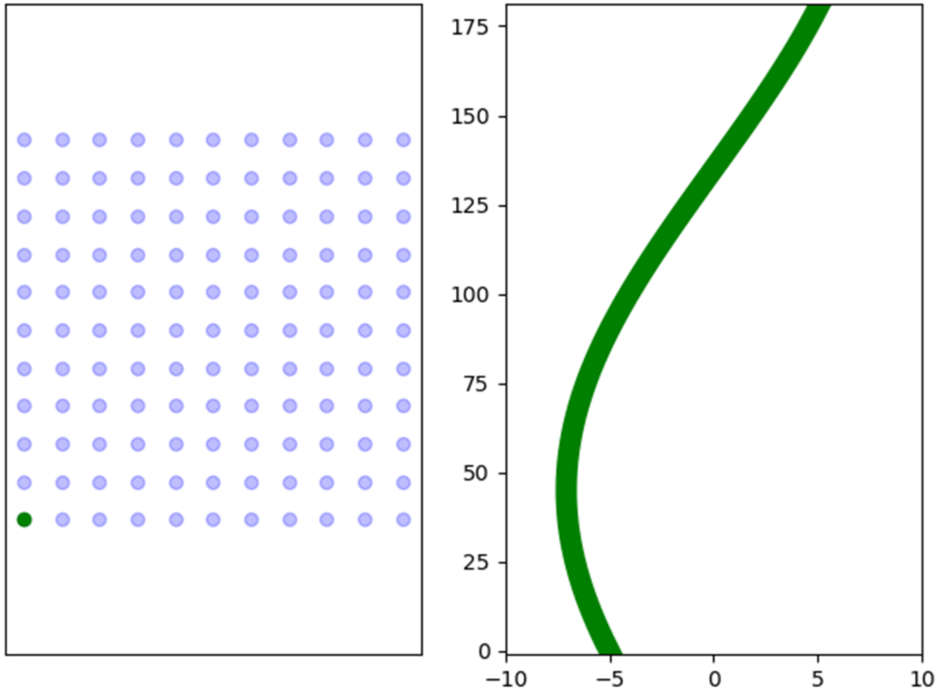

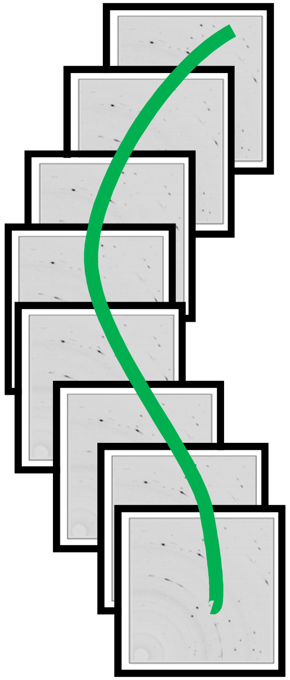

Measuring N steps across sample

N^2 possible data sets

(cross talk problem, but single crystal spots less overlapped)

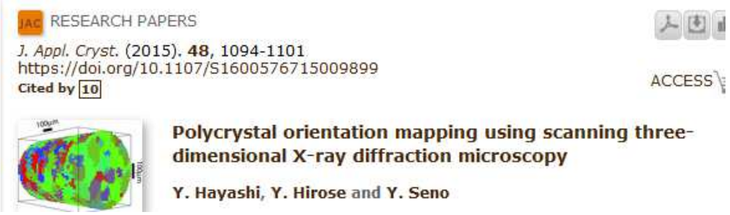

RESEARCH PAPERS

J. Appl. Cryst. (2015). **48**, 1094-1101
https://doi.org/10.1107/S1600576715009899
Cited by 10

ACCESS

Polycrystal orientation mapping using scanning three-dimensional X-ray diffraction microscopy

Y. Hayashi, **Y. Hirose** and **Y. Seno**

Diffraction tomography: Impurities in UMo (data from ID22)

Data reduction is well established for powder rings

“Spotty” diffraction patterns are more challenging to reconstruct.

Indexing of single grains has been achieved, showing orientation relations of phases

Impurity precipitation in atomized particles evidenced by high resolution diffraction tomography

Anne Bonnin, Jonathan Wright, Rémi Tucoulou, and Hervé Palancher
APPLIED PHYSICS LETTERS 104, 121910 (2014)

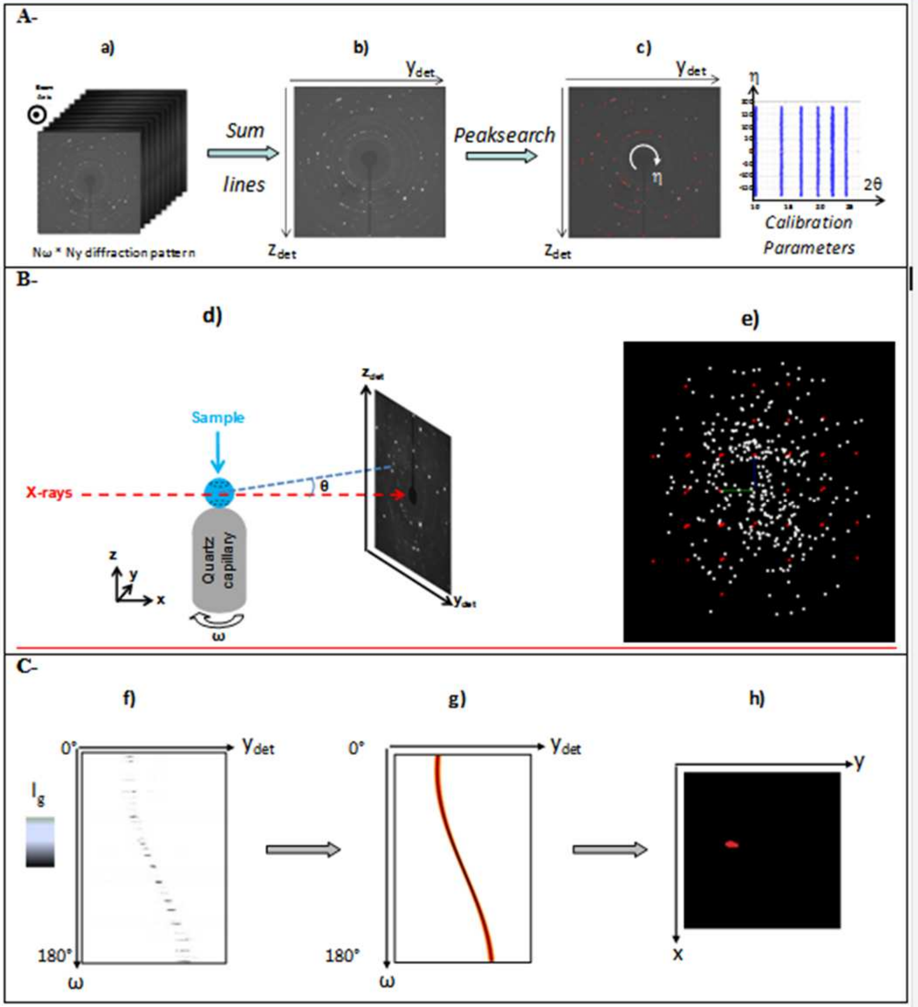

Index individual spots and reconstruct grain shapes

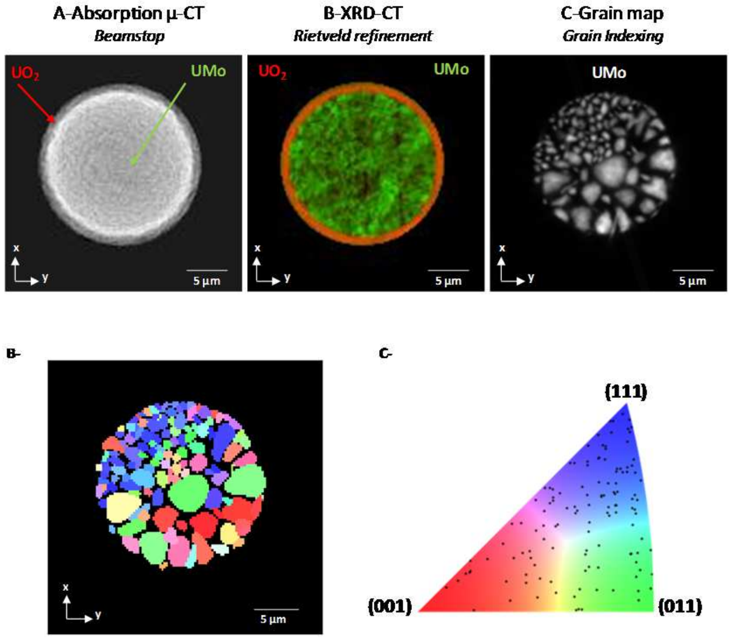

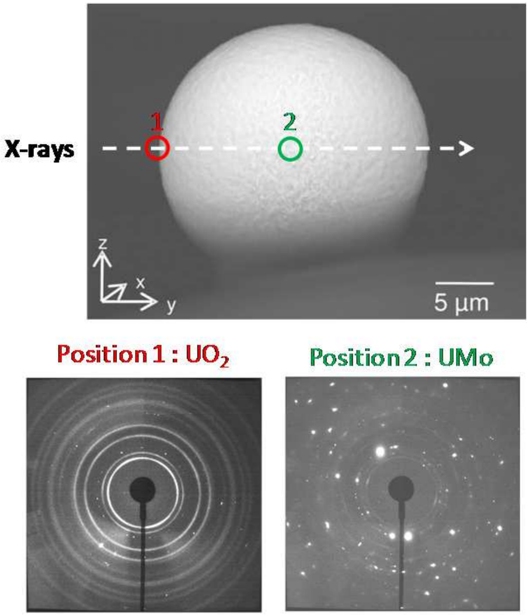

Impurity precipitation in atomized particles evidenced by high resolution diffraction tomography
Anne Bonnin, Jonathan Wright, Rémi Tucoulou, and Hervé Palancher, APL 2014

Similar grain in DCT experiment at ID11

ID11 near-field data

Processed for grain centre of mass

LARGE beamsize

Same size gradient but no U/C

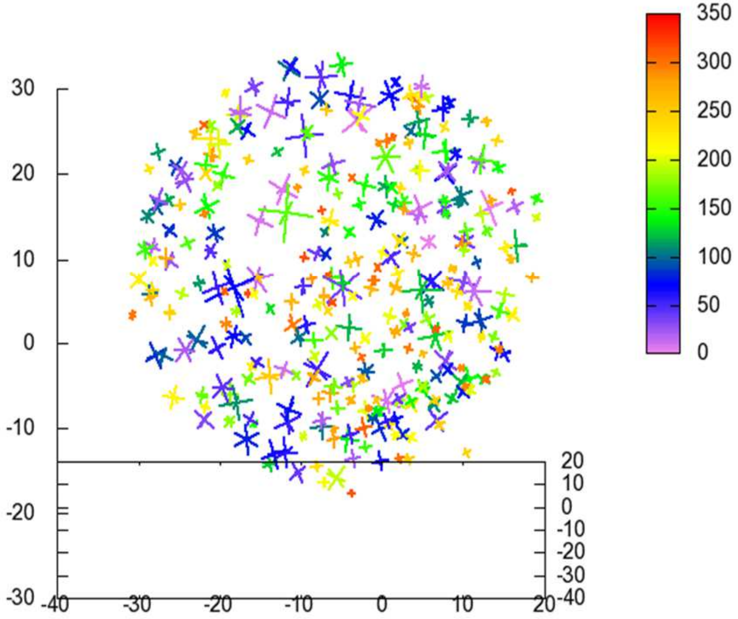

Trace impurity phase mapped out

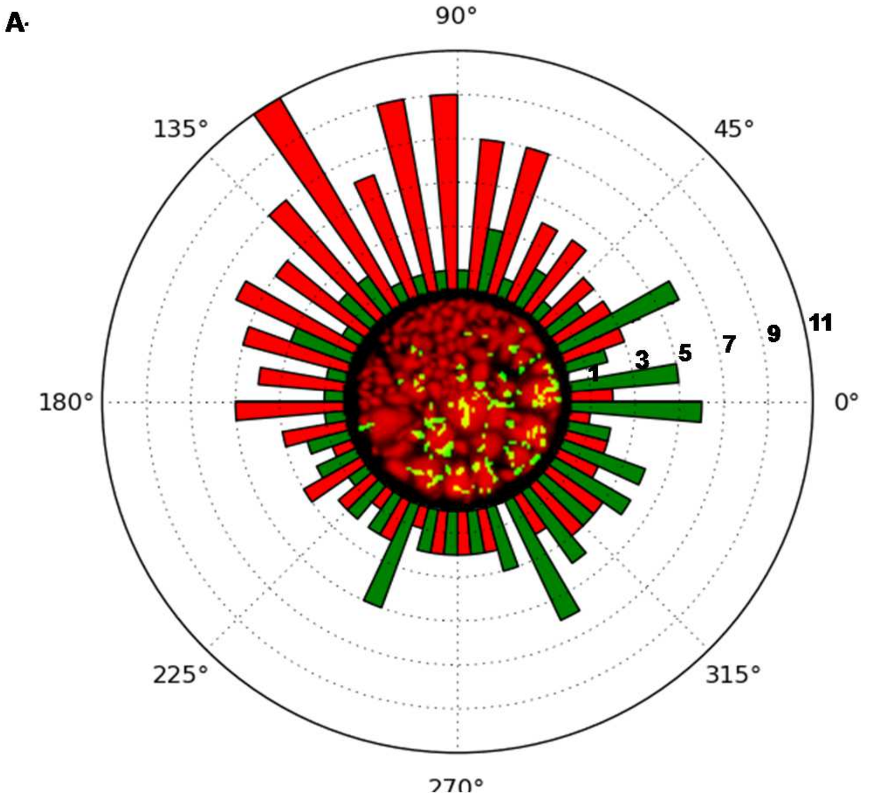

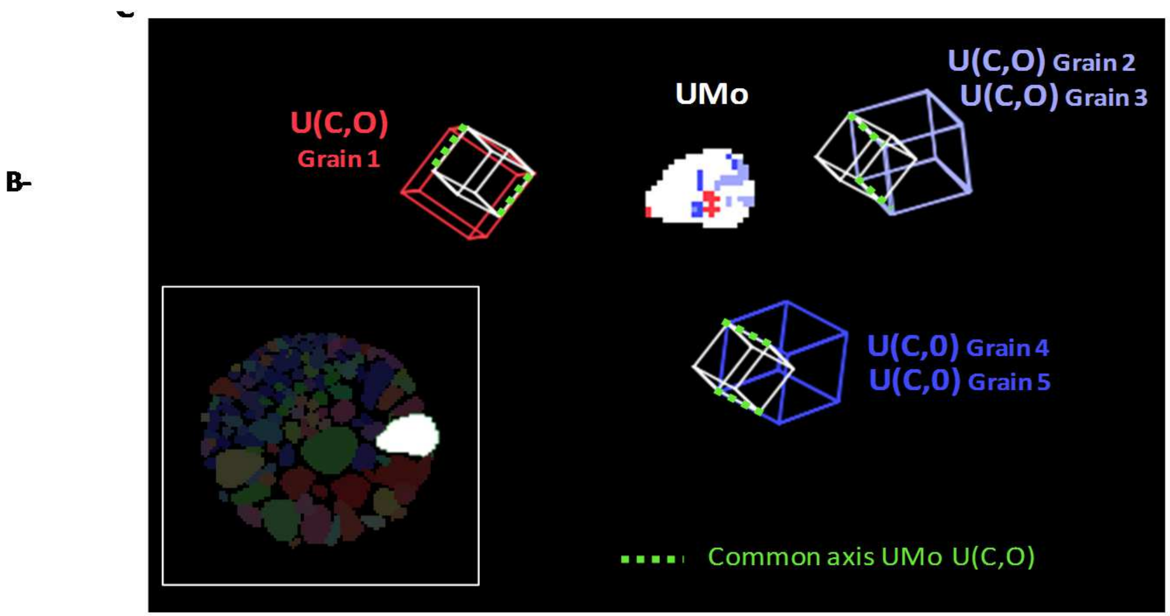

1 wt% impurity phase
Clear orientation relationship between U(C,O) and UMo
Multiple U(C,O) domains in single UMo grain
Mainly found in larger UMo grains

Bonnin *et al* APL 2014

Commissioning results from ID11, LTP, ma1317

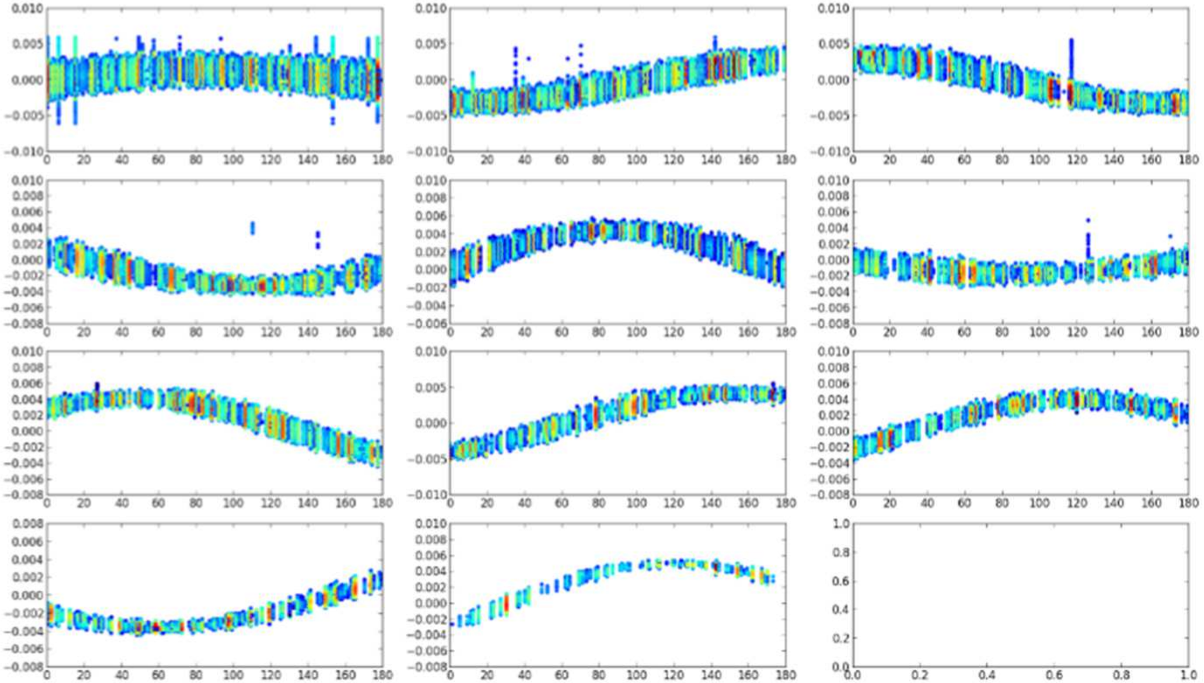

Grain by grain sinograms

YSZ sample

Jacob Bowen,
Jette Oddershede,
Soeren Schmidt,
Carsten Gundlach,
Hugh Simons

DTU

Layer by layer reconstruction

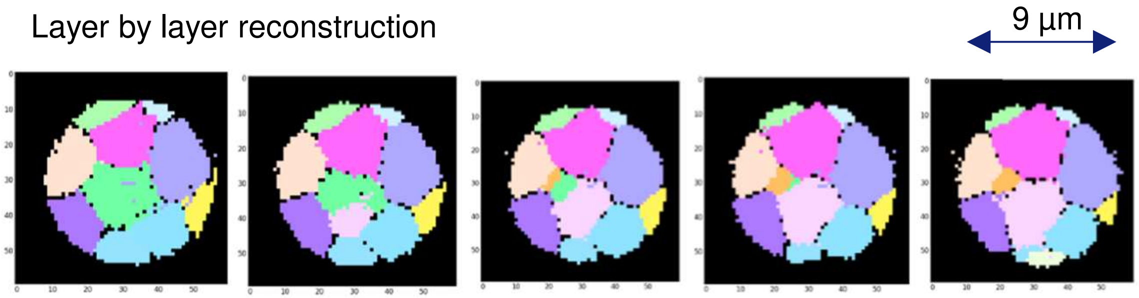

Scanning 3DXRD Measurement of Grain Growth, Stress, and Formation of Cu_6Sn_5 around a Tin Whisker during Heat Treatment

Johan Hektor [1,*], Stephen A. Hall [1,*], N. Axel Henningsson [1], Jonas Engqvist [1],
Matti Ristinmaa [1], Filip Lenrick [2] and Jonathan P. Wright [3]

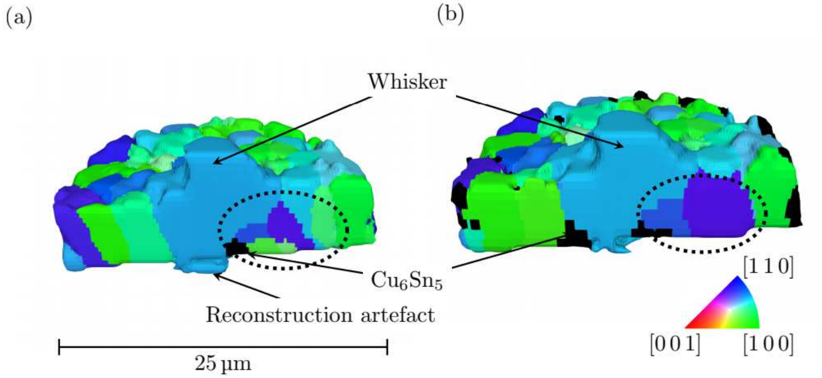

Figure 4. 3D reconstruction of the microstructure of the tin coating, the volume is sliced to reveal the columnar structure of the tin grains and the Cu_6Sn_5-grains situated below the whisker. The grains are coloured based on the crystal direction parallel to the sample normal: **(a)** before heat treatment; and **(b)** after heat treatment of 150 °C for three hours.

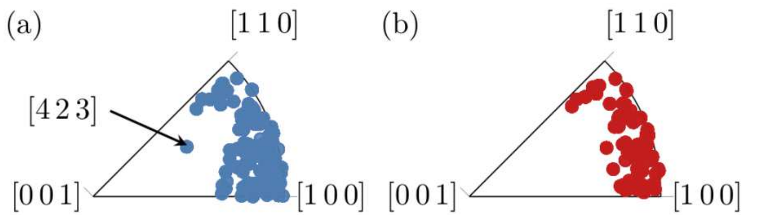

Figure 5. Inverse pole figure showing the crystal orientation parallel to the *z*-axis (sample normal). For reference to the coordinate system see Figure 2. The black arrow marks an orientation which is not present after the heat treatment: **(a)** before heat treatment; and **(b)** after heat treatment.

Materials **2019**, *12*, 446; doi:10.3390/ma12030446

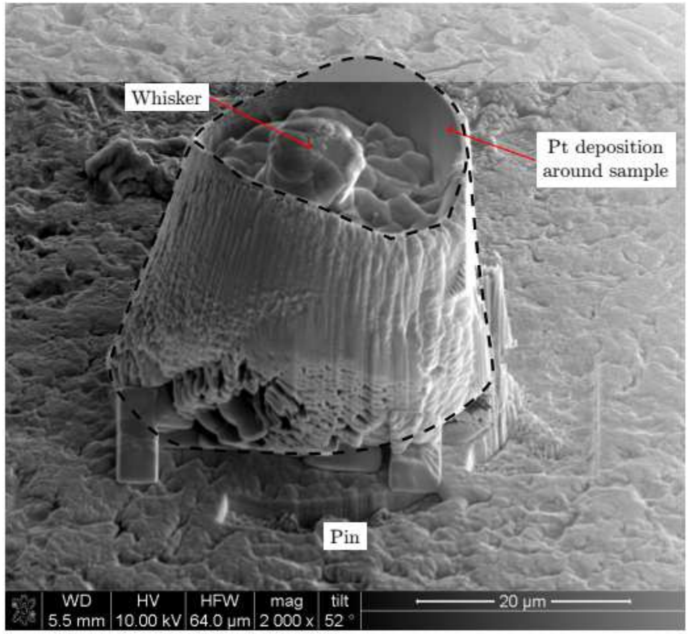

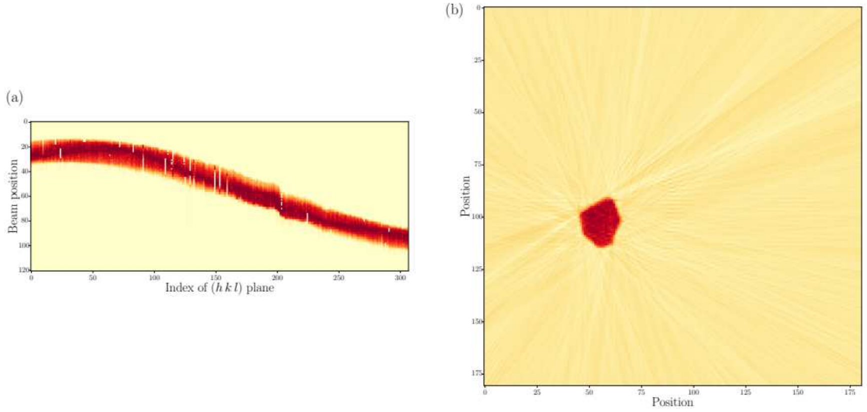

Figure 3. **(a)** Sinogram of one tin grain: The sinogram shows the sum of the intensities of all diffraction peaks belonging to the specific grain as a function of the diffracting lattice planes and the beam coordinate, *y*. The rows of the sinogram are normalised by the maximum intensity at each beam position. **(b)** Grain shape and position for one grain reconstructed by the inverse Radon transform of the sinogram.

Tin Whisker : Hektor et al…

“Low Angle Coincident Site Lattice”
“High Angle Coincident Site Lattice”

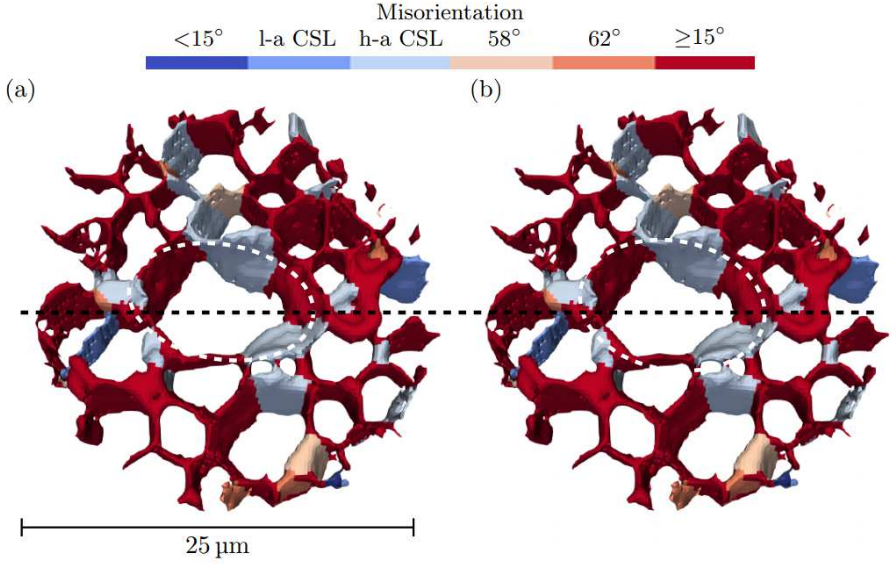

Figure 8. 3D renderings of the grain boundary network before and after heat treatment. The grain boundaries are coloured based on their misorientation angle. Blue and light blue represent low-angle CSL (l-a CSL) and high-angle CSL (h-a CSL) boundaries, respectively. The dashed ellipses indicate the location of the whisker. The dashed black line indicates where the volume in Figure 4 is sliced: (**a**) before heat treatment; and (**b**) after heat treatment.

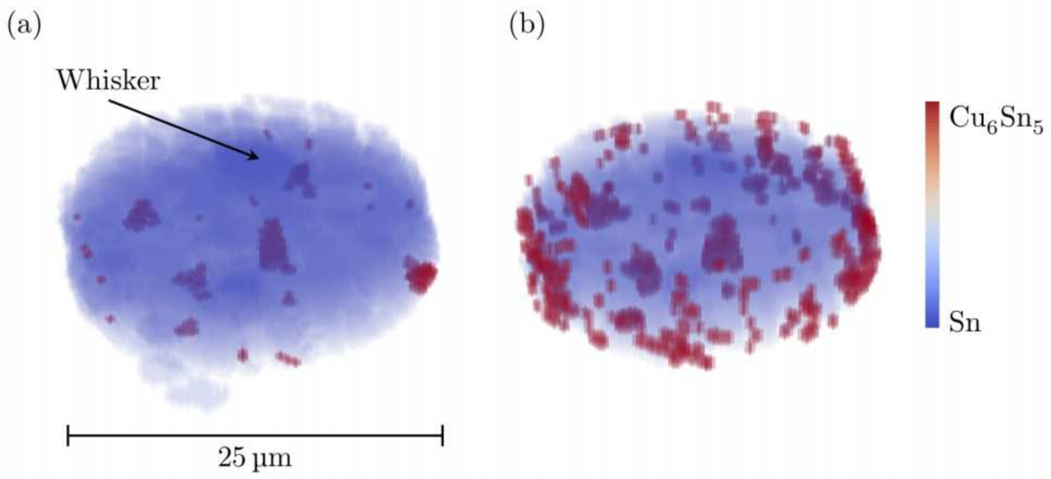

Figure 10. 3D map showing the location of Cu_6Sn_5 grains (red) in the Sn coating (blue): (**a**) before heat treatment; and (**b**) after heat treatment of 150 °C for three hours.

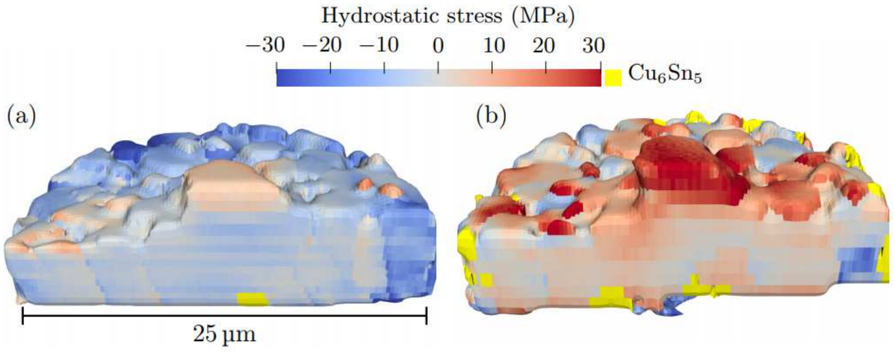

Figure 12. 3D reconstruction of hydrostatic stress field in the tin coating; the volume is sliced to reveal the internal structure. The stresses are calculated using the mean lattice parameters of the whisker as a stress-free reference. Yellow colour indicates Cu_6Sn_5: (**a**) before heat treatment; and (**b**) after heat treatment of 150 °C for three hours.

Steps for scanning 3DXRD processing

Peak search

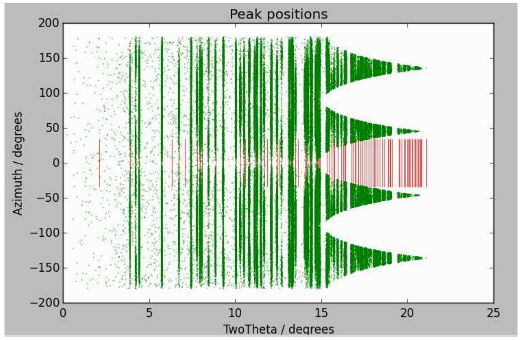

Calibrate

```
Ring assignment array shape (199088,)
Ring      (  h,   k,   l) Mult  total indexed to_index  ubis  peaks_per_ubi
…
Ring 8    ( -1,   0,  -3)   12   5446     254     5192   340     16
Ring 7    ( -1,  -1,  -1)   12     30       0       30     1     16
Ring 6    ( -1,  -1,   0)    6   2672      90     2582   334      8
Ring 5    (  0,   0,  -3)    2     28       2       26    10      2
Ring 4    ( -1,   0,  -2)   12   4830     296     4534   301     16
Ring 3    ( -1,   0,  -1)   12   4510     144     4366   281     16
Ring 2    (  0,   0,  -2)    2   1244      18     1226   466      2
Ring 1    ( -1,   0,   0)    6   2415     135     2280   301      8
```

3D scattering vectors.
Assign hkl indices
… for each crystallographic phase

Find orientation matrices and assign spots to grains

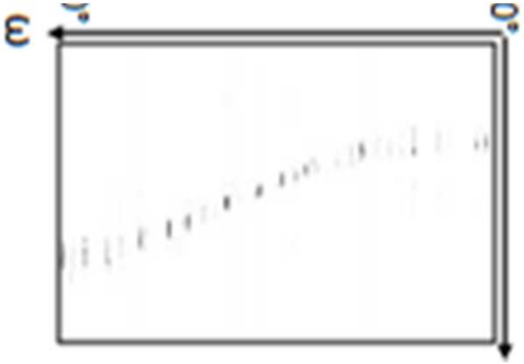

Map out the shape of the grain using filtered back projection or ART
(e.g. iradon function)

http://github.com/FABLE-3DXRD

What about the spots ? Event based integration

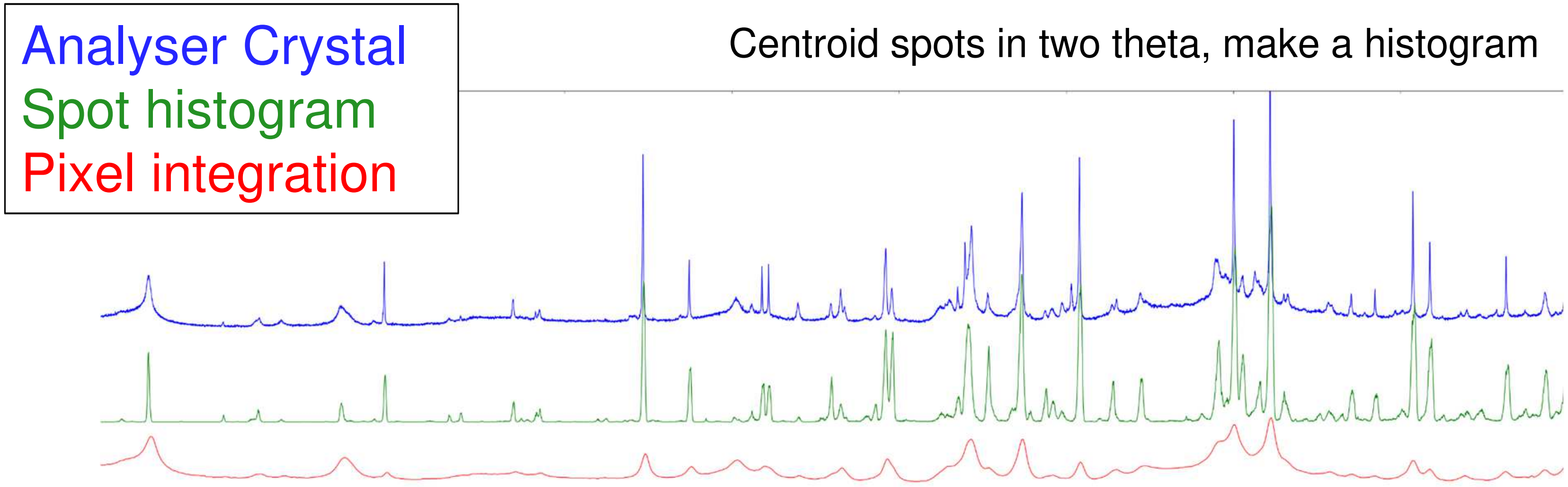

Centroid spots in two theta, make a histogram

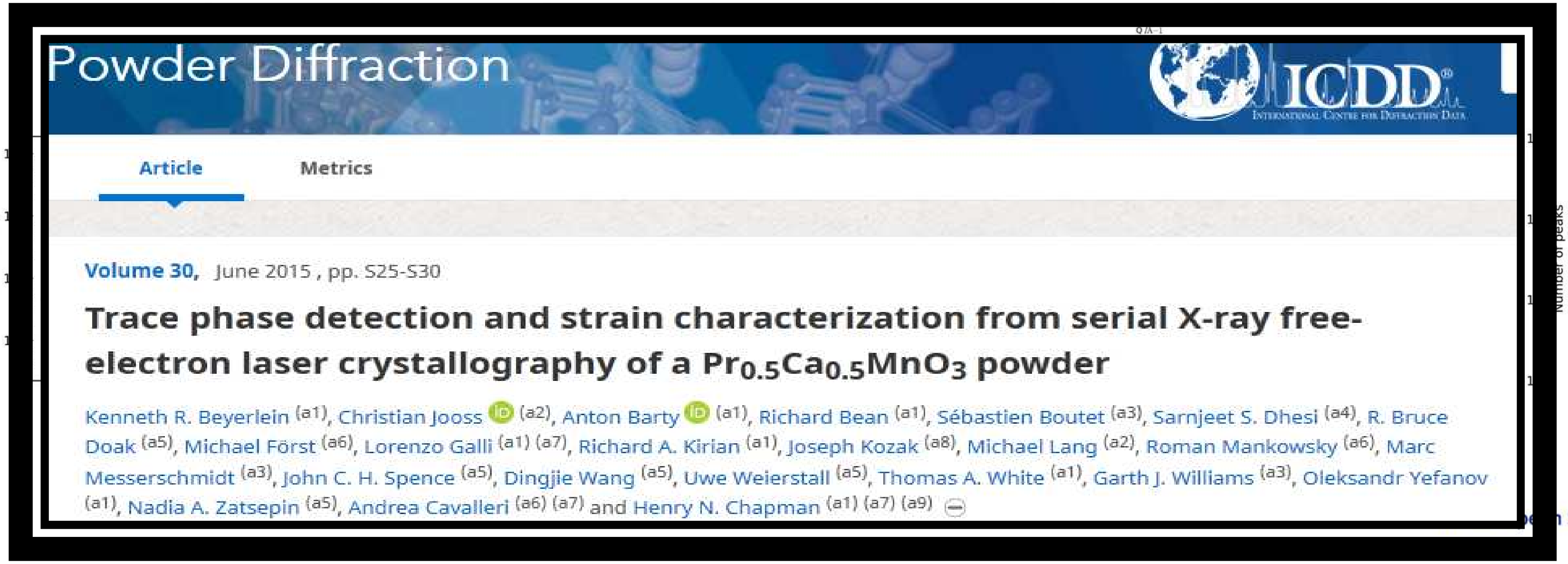

Volume 30, June 2015 , pp. S25-S30

Trace phase detection and strain characterization from serial X-ray free-electron laser crystallography of a $Pr_{0.5}Ca_{0.5}MnO_3$ powder

Kenneth R. Beyerlein (a1), Christian Jooss (a2), Anton Barty (a1), Richard Bean (a1), Sébastien Boutet (a3), Sarnjeet S. Dhesi (a4), R. Bruce Doak (a5), Michael Först (a6), Lorenzo Galli (a1) (a7), Richard A. Kirian (a1), Joseph Kozak (a8), Michael Lang (a2), Roman Mankowsky (a6), Marc Messerschmidt (a3), John C. H. Spence (a5), Dingjie Wang (a5), Uwe Weierstall (a5), Thomas A. White (a1), Garth J. Williams (a3), Oleksandr Yefanov (a1), Nadia A. Zatsepin (a5), Andrea Cavalleri (a6) (a7) and Henry N. Chapman (a1) (a7) (a9)

Summary

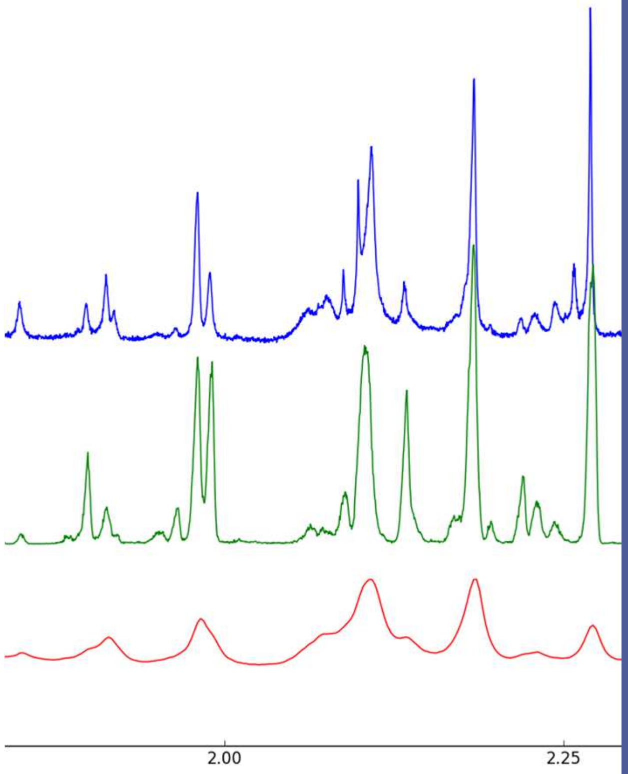

Un-mixing samples

- phase pure voxel data

Single crystals from powders

- tiny x-ray beams
- search all over to find crystals

Event based integrations

- two theta of spots

Computed Tomo is like a sample changer

- > 10,000 positions

Acknowledgements

ESRF
Thomas Buslaps
Carlotta Giacobbe
Marta Majkut
Pavel Sedmak
Wolfgang Ludwig
Nicola Vigano
Henri Gleyzolle
Ludovic Ducotte
Emmanuel Papillon
Jose-Maria Clement
Jerome Kieffer

Tin Whisker

Johan Hektor
Steve Hall
Axel Henningsson

Force Chains
Steve Hall
Ryan Hurley

UMo
Anne Bonnin
Herve Palancher
Remi Tucoulou

Thank you for listening.

See you in Grenoble?

Cement
Francis Claret
Sylvain Grangeon
Nick Harker

Event Histograms
Agnès Elmaleh